# Complement C5a receptor 1 blockade reverses cognitive deficits following cranial radiation therapy for brain cancer

Robert P. Krattli[1,*], An H. Do[1,*], Sanad M. El-Khatib[1], Leila Alikhani[1], Mineh Markarian[1], Arya R. Vagadia[1], Manal T. Usmani[1], Shreya Madan[1], Janet E. Baulch[2], Richard J. Clark[3], Trent M. Woodruff[3], Andrea J. Tenner[4], Munjal M. Acharya[1,§]

[1]Department of Anatomy & Neurobiology, University of California Irvine, United States.
[2]Department of Radiation Oncology, University of California Irvine, United States.
[3]School of Biomedical Sciences, The University of Queensland, St Lucia, Brisbane, Australia.
[4]Department of Molecular Biology & Biochemistry, University of California Irvine, United States.

*Contributed equally

**[§]Corresponding author:**
Dr. Munjal M. Acharya
Associate Professor
Department of Anatomy and Neurobiology,
Department of Radiation Oncology (Joint),
School of Medicine, University of California, Irvine
Email: macharya@uci.edu

**The authors declare no relevant conflicts of interest or financial relationships.**

**Keywords:** Complement cascade, C5a, C5aR1, PMX205, neuroinflammation, cognitive function, radiation therapy, brain cancer

**ABSTRACT**

Cranial radiation therapy (RT) for brain cancers leads to an irreversible decline in cognitive function without an available remedy. Radiation-induced cognitive deficits (RICD) are particularly a pressing problem for the survivors of pediatric and low grade glioma (LGG) patients who often live long post-RT. Radiation-induced elevated neuroinflammation and gliosis, triggered by the detrimental CNS complement cascade, lead to excessive synaptic and cognitive loss. Using intact and brain cancer-bearing mouse models, we now show that targeting anaphylatoxin complement C5a receptor (C5aR1) is neuroprotective against RICD. We used a genetic knockout, C5aR1 KO mouse, and a pharmacologic approach, employing the orally active, brain penetrant C5aR1 antagonist PMX205, to reverse RICD. Irradiated C5aR1 KO and WT mice receiving PMX205 showed significant neurocognitive improvements in object recognition memory and memory consolidation tasks. C5aR1 inhibition reduced microglial activation, astrogliosis, and synaptic loss in the irradiated brain. Importantly, C5aR1 inhibition in the syngeneic, orthotopic astrocytoma, and glioblastoma-bearing mice protected against RICD without interfering with the therapeutic efficacy of RT to reduce tumor volume *in vivo*. PMX205 is currently in clinical trials for amyotrophic lateral sclerosis (ALS). Thus, C5aR1 inhibition is a translationally feasible approach to address RICD, an unmet medical need.

## INTRODUCTION

Despite being effective for tumor control, cranial radiation therapy (RT) for treating primary and metastatic brain cancers causes an unintended and irreversible impact on brain function, including cognitive impairments[1]. Long-term sequelae of radiation-induced cognitive impairments (RICD) are particularly crucial for childhood brain cancer and low grade glioma (LGG) survivors who often live long post-therapy[2]. RT triggers a CNS cascade of immune and non-immune consequences, including detrimental activation of complement cascade[3,4], leading to long-term microglial activation and the loss of synaptic integrity that eventually culminate in RICD[3]. The CNS complement cascade plays unique roles in the neural stem cell polarity determination[5] and pruning and maintaining the synaptic landscape during brain development[6]. However, under pathological conditions, including Alzheimer's disease (AD), traumatic brain injury (TBI), and RICD, excessive complement cascade activation promotes neurodegeneration via elevated neuroinflammation[3,6]. We have shown that microglia-selective knockdown of an upstream complement C1q was neuroprotective against RICD, microglial and astrocytic activation, synaptic loss, and anaphylatoxin C5a receptor 1 (C5aR1) expression[3]. C1q also plays an essential role in pruning synapses in the CNS[6]; thus, the ablation of the upstream complement activation node might not be the optimal therapeutic approach to prevent RICD.

The genetic knockdown or pharmacologic inhibition of C5aR1 significantly reduced AD neuropathologies, including plaques, gliosis, and hippocampal-dependent cognitive dysfunction[7-9]. On the contrary, C5a overexpression in the brain worsened hippocampal memory[10]. C5a-C5aR1 signaling inhibition using a highly selective, BBB-permeable, cyclic hexapeptide antagonist, PMX205[11], significantly reduced microglial pro-inflammatory polarization, inflammatory gene expression, and excessive synaptic loss in AD brain[8,9,12]. Notably, an FDA-approved C5aR1 antagonist, Avacopan, is safe, well-tolerated, and effective against autoimmune disease[13], suggesting that C5aR1 inhibition can be a viable and safe strategy against RICD. PMX205 is under Phase I clinical trial to treat ALS (trial ref. ACTRN126490016391). Interestingly, C5a signaling has been suggested to increase tumorigenesis in colorectal, gastric, and ovarian tumors and glioma stem-like proliferation[14-17]. C5aR1 inhibition using PMX205 has also improved the therapeutic efficacy of RT with minimal normal tissue damage in GIT cancers[18].

Cranial RT-induced CNS complement cascade activation can lead to long-term inflammatory injury and synaptic loss in the irradiated brain[3,6]. Therefore, tractable approaches to block pro-inflammatory C5a-C5aR1 signaling without altering the therapeutic efficacy of cranial RT for brain cancers need to be investigated. The current study provides evidence that genetic KO and pharmacological C5aR1 blockade prevent cranial RT-induced gliosis and synaptic loss

and ameliorate RICD. Notably, the C5aR1 blockade did not interfere with the therapeutic efficacy of RT in two glioma models, increasing the translational significance of this strategy.

## RESULTS

**<Figure 1>**

*Inhibition of the C5a-C5aR1 axis ameliorates RT-induced cognitive impairments.*

To determine if C5aR1 inhibition impacts RICD, we tested transgenic and pharmacologic approaches, including a C5aR1 knockout (C5aR1-KO) and an orally active C5aR1 antagonist, PMX205, respectively. KO mice were generated by targeted gene deletion (a kind gift from R. A. Westel)[19]. WT (C57Bl6) and C5aR1-KO mice were exposed to 9 Gy cranial RT with the protection of eyes and cerebellum as described in the **Methods** and **Fig. 1A**. At 48h post-RT, WT mice received PMX205 treatment (20 µg/ml, or 100 µg per day) in the drinking water for 1-month. In addition, mice were injected with PMX205 (1 mg/kg, SQ) for the first 7-days of the antagonist treatment. To confirm the genetic KO of C5aR1, qPCR and flow cytometry analyses (**Suppl. Fig. S1**) of C5aR1 (CD88) expression in the C5aR1-KO mice brains and blood showed nearly complete knockdown (>96-98%) in the 0 and 9 Gy irradiated animals. At one-month post-irradiation, all cohorts of mice (WT mice, 0 and 9 Gy ±PMX205; C5aR1-KO mice ±9 Gy) were habituated and tested on the cognitive function tasks. During the open field activity, no significant differences were found between the animal groups for the percentage of time spent in the central area (30% of the total area, **Suppl. Fig. S2A**), indicating spontaneous exploration and the absence of neophobic behavior during cognitive testing. Similarly, the percentage of time spent in the open arms did not vary significantly between the groups in the elevated plus maze task (**Suppl. Fig. S2B**). After three days of habituation, animals were administered the object recognition memory (ORM) task. During the test phase, the total time exploring both familiar and novel objects was comparable between each experimental group. This behavior is apparent in the heat map of animal exploration depicting the activity for the novel or familiar objects (**Fig. 1B**). No difference was detected in the memory index of 0 Gy WT mice, WT mice +PMX205 or C5aR1-KO mice. As expected, 9 Gy WT mice showed a significant decline in the memory index (novel object exploration preference) compared to unirradiated (0 Gy) WT control (**Fig. 1C**, $P<0.0001$). This decline was prevented in irradiated WT+PMX205 and C5aR1-KO mice (**Fig. 1C**, $P<0.01$, $P<0.001$, respectively). The performance for the object location memory (OLM) task showed an RT-induced decline in the memory index in the 9 Gy WT mice compared to the 0 Gy WT ($P<0.05$, **Fig. 1D**). Treatment with PMX205 to the irradiated WT mice significantly improved the memory index compared to the 9 Gy WT group ($P<0.01$). C5aR1-KO mice receiving either 0 or 9 Gy cranial

RT showed a trend in improvements on the memory index, albeit it did not reach statistical significance. Nonetheless, the behavior of 0 Gy and 9 Gy exposed C5aR1-KO mice was comparable to the 0 Gy WT mice group. Lastly, to evaluate the impact of cranial RT and C5aR1 inhibition on the hippocampal-amygdala fear memory consolidation circuit, mice were administered a fear extinction test reliant on hippocampal function[20,21]. Irradiated WT mice showed a significantly elevated freezing behavior, an indicator of disrupted memory consolidation processes, compared to the 0 Gy WT mice (P<0.0003, **Fig. 1E**). The freezing behavior of 0 Gy WT+PMX205 and 0 Gy C5aR1-KO mice was comparable to the 0 WT controls. 9 Gy WT mice+PMX205 and 9 Gy C5aR1-KO mice showed reduced freezing compared to 9 Gy WT mice (P<0.003, P<0.05, respectively, **Fig. 1E**). In summary, genetic knockdown and pharmacologic inhibition of the C5a-C5aR1 axis protect against RICD.

**<Figure 2>**

*C5aR1 inhibition reduced neuroinflammation.*

To determine if C5aR1 inhibition (PMX205) in the WT mice prevented radiation-induced neuroinflammation, surrogate markers of RT-induced gliosis and complement anaphylatoxins were evaluated using immunofluorescence staining and 3D algorithm-based volumetric quantification of immunoreactivity. Cranial RT significantly elevated microglial lysosomal phagocytosis marker CD68 (CD68-IBA1, **Fig. 2A-C**) in the 9 Gy+Vehicle brains compared to 0 Gy+Vehicle group (P<0.0001). 0 Gy and 9 Gy mice +PMX205 treatment showed significantly lower CD68-IBA1 compared to the 9 Gy+Vehicle group (P's<0.001, **Fig. 2C**). Microglial C5aR1 expression was significantly elevated in the WT 9 Gy+Vehicle brains compared to the 0 Gy+Vehicle, 0 Gy+PMX205 and 9 Gy+PMX205 groups (P's<0.001, **Fig. 2D-F**). PMX205 treatment to the 9 Gy irradiated animals reduced microglial-C5aR1 expression compared to 9 Gy+Vehicle (P<0.001). Moreover, cranial RT significantly elevated astrocytic-C3 immunoreactivity (GFAP-C3d) in the 9 Gy+vehicle brains compared to 0 Gy+Vehicle group (P<0.03, **Fig. 1G-H**). The astrocytic-C3 expression and astrogliosis did not differ between 0 Gy+Vehicle and 0 Gy+PMX205 groups. 9 Gy+PMX205 mice had significantly reduced GFAP-C3 immunoreactivity compared to the 9 Gy+Vehicle group (P<0.02, **Fig. 2H**). Thus, C5aR1 inhibition prevented cranial RT-induced microglial activation and astrogliosis that was coincident with neurocognitive improvements.

**<Figure.3>**

*C5aR1 inhibition prevented RT-induced disruption of synaptic integrity.*

Microglial and complement cascade activation have been shown to play detrimental roles in excessive synaptic loss in neurodegenerative conditions, including RICD[3,6]. To determine the impact of C5aR1 blockade using PMX205 on the synaptic integrity in the irradiated WT brain, we quantified immunoreactivity of post- and pre-synaptic markers PSD95 and synaptophysin, respectively (**Fig. 3**). Previously, we reported that RT elevates PSD95 in the mice brains that were cognitively impaired[22,23]. Likewise, in this study, we found elevated PSD95$^+$ in the irradiated hippocampal molecular layer (9 Gy+Vehicle) compared to 0 Gy+Vehicle and 0 Gy+PMX205 groups (P<0.0001, P<0.001 respectively, **Fig. 3A-B**). PMX205 treatment showed a significant PSD95 reduction in the 9 Gy+PMX205 compared to 9 Gy+Vehicle brains (P<0.0001). In contrast, RT significantly reduced synaptophysin$^+$ puncta compared to the 0 Gy+Vehicle group (P<0.0001, **Fig. 3C-D**). The synaptophysin levels were comparable between the 0 Gy and 9 Gy mice +PMX205. Irradiated mice receiving PMX205 did not show reduced synaptophysin compared to the 9 Gy+vehicle group (P<0.0001). Overall, these data indicate a protective role of C5aR1 inhibition against RT-induced disruption of synaptic integrity.

**<Figure 4>**

*PMX205 treatment prevented RICD in the brain cancer-bearing mice without interfering with the therapeutic efficacy of RT*

Cranial RT is the primary treatment modality to stall the brain cancer progression. The impact of C5aR1 inhibition on the WT brain cancer growth, overall survival, and cognitive function post-RT was tested using orthotopic glioblastoma multiforme (GBM) and astrocytoma models. WT mice received intra-cranial injection of syngeneic murine Gl261 or CT2A-luc$^+$ cells to model glioblastoma and astrocytoma, respectively (Research design, **Fig. 4A**). 1-week post-tumor induction and detection via imaging, mice received 9 Gy brain-RT. A cohort of mice also received PMX205 treatment (1 mg/kg SQ for one week concurrently with 20 µg/ml in the drinking water). For 4-5 weeks post-tumor induction, tumor growth, tumor burden, and animal health status were monitored, followed by the object recognition memory (ORM) behavior test. Gl261 implanted mice showed a steady tumor growth as detected by the iodine contrast CBCT (**Fig. 4B**). We found a trend for reduction in the tumor growth at 4-5 weeks post-PMX205 and RT (9 Gy)+PMX205 treatments, albeit it did not reach the statistical significance. Conversely, CT2A-luc showed a rapid and steady tumor progression as detected by the BLI (**Fig. 4C**). At 4-weeks post-implantation, we found a significant reduction (P's<0.002) in the tumor burden following 9 Gy RT and PMX205

treatments (CT2A+RT, CT2A+PMX205, and CT2A+RT+PMX205) compared to the CT2A+Vehicle group.

The Kaplan-Meier survival curves for the Gl261 mouse model showed improved survival rates for the GBM-bearing mice receiving RT or RT+PMX205 treatments compared to GBM mice treated with vehicle or PMX205 (P's<0.0001, **Fig. 4D**). On an average, survival for Gl261-bearing mice receiving RT or RT+PMX205 treatments was 54-60 days, whereas, vehicle or PMX205 treatment alone did not influence the survival beyond 36-39 days post-tumor induction. Contrary to this, the CT2A-luc-implanted astrocytoma model did not show significant improvements in survival following RT alone, PMX205 alone, or RT+PMX205 treatments, and the average survival was between 35-40 days post-tumor induction (**Fig. 4E**).

Concurrently, at 3-4 weeks post-RT, the neurocognitive function (ORM) was assessed on the brain cancer-bearing mice with or without PMX205 treatment (**Fig. 4F**). For reference, ORM data for *No Tumor* mice was derived from **Fig. 1C**. Tumor burden significantly reduced the performance on ORM task for both Gl261+Vehicle and CT2A+Vehicle groups compared to Control+Vehicle group (P's<0.01, **Fig. 4F**, glioblastoma and astrocytoma groups). Cancer bearing-mice receiving RT (Gl261+RT and CT2A+RT) also performed poorly on the ORM task (P's<0.01) versus Control+Vehicle group. Importantly. Gl261- and CT2A-bearing mice +PMX205 showed significantly improved memory index compared to Gl261- and CT2A-bearing mice +vehicle (P<0.0001, P<0.02 respectively, **Fig. 4F**). Remarkably, PMX205 treatment significantly improved memory indices for the brain cancer-bearing mice receiving RT. The performance of Gl261+RT+PMX205 and CT2A+RT+PMX205 mice was significantly higher compared to Gl261+RT and CT2A+RT groups (P's<0.02). Thus, PMX205 treatment was neuroprotective in brain cancer-bearing mice receiving RT.

## DISCUSSION

RICD, prevalent in 50-90% of surviving brain cancer patients, has long been recognized as adversely afflicting their overall quality of life (QOL)[24]. Yet, neither the neurobiological mechanisms driving such poor neurocognitive outcomes nor preventative measures are well developed. Despite extensive knowledge of aberrant complement activation in neurodegenerative conditions, specific consequences of the C5a-C5aR1 axis in the irradiated and cancer-bearing brain are not yet reported. RT-induced microglial activation plays a pivotal damaging role in leading to a cascade of pro-inflammatory events, including CNS complement activation[3,6]. The current study seeks to understand the detrimental role of the downstream complement C5a signaling. C5a is an anaphylatoxin and a product of complement cascade activation via cleavage

of C5. It has been shown to stimulate chemotaxis and a robust pro-inflammatory response after interaction with C5aR1[6]. Activation of the C5a-C5aR1 axis promotes pro-inflammatory polarization of microglia, excessive synaptic pruning, and loss of cognitive function in AD models[7,9]. C5a overexpression in AD mice led to accelerated hippocampal-dependent memory loss[10]. Contrarily, genetic KO or selective C5aR1 inhibition protected the AD brain against microglia-mediated excessive synaptic loss, improved neuronal function, and reduced dementia[7,9,25]. These reports established the detrimental role of the C5a-C5aR1 axis in promoting cognitive decline in a chronic neurodegenerative condition. Cranial RT led to a similar extent of microglial activation, synaptic loss, and cognitive decline (sans plaque deposition) in the brain[3,22,26,27]. Cranial RT-induced cognitive impairments were linked with elevated microglial activation, astrocytic hypertrophy, and elevated pro-inflammatory cytokines *in vivo*[26,28,29]. Subsequently, microglia elimination or reduced astrogliosis reversed those cognitive deficits[26,30]. CNS complement components are co-localized or expressed by both microglia and astrocytes *in vivo*, and they synchronize pathologic response and normal tissue toxicity in the irradiated brain.

We seek to understand an overarching issue if RT-induced neuropathologic condition in an intact, cancer-free mice brain leads to the activation of the classical complement cascade and formation of anaphylatoxin that steers microglial and astrocytic activation, leading to the excessive synaptic alterations and RICD. To prove the principle, we tested two approaches, genetic C5aR1 KO and pharmacologic inhibition, using a selective, orally active inhibitor, PMX205. Exposure to an acute 9 Gy cranial RT led to a significant disruption in hippocampal, frontal cortex, and amygdala-dependent learning and memory and memory consolidation and re-learning processes (**Fig. 1**). In the past, we have shown that such neurocognitive disruptions are often progressive, persistent for as long as 8-months post-RT and do not resolve over a time[28,31]. RICD was more pronounced in the fear extinction memory that measures the memory consolidation process, an ability to re-learn or dissociate from a previously aversive experience. Importantly, PMX205 significantly reduced RICD. Comparable results in the C5aR1 KO mice asserted the selective specificity of our pharmacologic C5aR1 inhibition approach. Irradiated C5aR1 KO mice did not show a cognitive decline compared to the irradiated WT mice. These data support our previous findings that show accelerated cognitive impairments following C5a overexpression[10] and that C5aR1 inhibition (PMX205) improved cognition in AD model[7]. Among the recent advances targeting complement activation post-RT, our work has shown that microglia-selective deletion of C1qa in the irradiated CNS prevented RICD and excessive synaptic loss[3]. Moreover, inhibition of complement receptor 3 (CR3) axis also reduced RICD[32]. Such inhibition of upstream complement C1q and C3 would prevent downstream events such as C5a generation C5aR1 signaling[3,6]. As

these upstream complement components play several beneficial roles, a complete ablation or inhibition of the CNS complement cascade may not be an optimal mitigation strategy for the irradiated brain. Instead, inhibition of the downstream anaphylatoxin C5a-C5aR1 signaling axis is a better approach to prevent microglial activation and the RICD.

In this study, we confirmed the status of microglial activation, microglial-C5aR1 expression, and astrogliosis by dual-immunofluorescence and 3D algorithm-based volumetric quantification[3] of immunoreactive cell surface or puncta and *in silico* modeling of colocalization post-C5aR1 inhibitor treatment in the irradiated brains (**Fig. 2**). Cranial RT-induced elevated microglial activation was characterized by increased expression of the lysosomal phagocytotic marker, CD68, by the $IBA^+$ microglia. The microglial C5a receptor (C5aR1-IBA1) expression was also elevated post-RT. The irradiated brains showed hypertrophic astrocytes co-labelled with C3d *in vivo*. Together, these markers are characteristic of gliosis in the irradiated brain. Treatment with PMX205 significantly reduced microglial activation and C5aR1 expression, and astrogliosis in irradiated brains. Concurrently, the assessment of synaptic proteins showed two opposite trends. RT significantly elevated PSD95 and reduced synaptophysin (**Fig. 3**), and conversely, irradiated brains treated with PMX205 showed restoration in this synaptic protein expression. These data corroborate our past findings that cranial RT exposure increased PSD95 and reduced synaptophysin expression[22]. PSD95 is a scaffolding protein that plays important roles in neuron and dendritic spine growth and maturation, yet, mutations and varied post-translational modifications in PSD95 are also linked with neurodevelopmental disorders[33,34]. Aging and neuroinflammation-related elevations in PSD95 were correlated with imbalanced excitatory to inhibitory synaptic circuits, leading to excitotoxic events and neuro-psychiatric disorders[35-37]. Cranial RT-induced elevated PSD95 was suggested to coincide with reduced dendritic branching, dendritic complexity, and reduced expression of presynaptic marker synaptophysin[38]. Our data showed restoration in the expression of these synaptic proteins in the RT+PMX205-treated brains. C5aR1 signaling is critical in complement-mediated microglial synaptic pruning in the AD brain[9]. Furthermore, analyses of Arctic (AD) mice brains either crossed with C5aR1 KO[7] or treated with PMX205[8] showed a shift in the microglial polarization to a less inflammatory, more phagocytic state that facilitated plaque clearance and reduced gliosis. The C5aR1 signaling axis regulates both microglial functions, complement-mediated synaptic pruning, and synaptic engulfment[7,39]. Elevated microglial C5aR1 expression in the irradiated brain also synergizes with TLR4 expression, DAMP response[3], and astrogliosis that polarizes microglia to an inflammatory and damaging state, leading to imbalanced synaptic function and thereby leading to RICD. Thus, C5a-C5aR1 axis inhibition will suppress the microglial pro-inflammatory polarization and promote

beneficial activity, including clearance of dead cell debris. Possibility that needs to be tested in the irradiated brain. In total, our data and the literature support a neuroprotective role the C5aR1 axis inhibition in alleviating neurodegenerative consequences post-RT.

The translational feasibility of this neuroprotective strategy against RICD and neuroinflammation needed to be tested in brain cancer. Cranial RT is a clinical treatment regimen for primary and metastatic CNS cancers. The detrimental CNS impact of RT, particularly for the long-term survivors of childhood brain cancer and LGG, reduces the QOL and thus limits the therapeutic outcome[1,42]. We tested the neuroprotective efficacy of C5aR1 inhibition on two syngeneic mouse brain cancer models, astrocytoma (CT2A cells) and glioblastoma (GBM, GL261 cells). Brain cancer-bearing mice receiving cranial RT showed dampened tumor growth compared to unirradiated mice (**Fig. 4**). PMX205 treatment of brain cancer-bearing mice ±RT did not significantly impact GBM growth. However, it reduced astrocytoma growth ±RT compared to the vehicle-treated mice. Syngeneic GL261 is an aggressive form of high-grade glioma that typically responds to high doses of fractionated RT and temozolomide treatments. In contrast, $CT2A^{+}$ astrocytoma showed a rapid initial growth and radiation response following an acute 9 Gy RT and PMX205 treatment. Nonetheless, cranial RT±PMX205 treatment improved survival in Gl261-bearing mice compared to the unirradiated cohort. We did not observe significant differences in survival for astrocytoma-bearing mice. Overall, these brain cancer data suggest that PMX205 treatment did not interfere with the therapeutic outcome of acute (9 Gy) cranial RT. Clinical studies have shown complement deposition (C3, C5b-9), and overexpression of C3aR in patient-derived GBM tissues[40,41]. Elevated complement components have been reported in vascularization and growth of malignant glioma[42]. Genetic ablation of C3a and C5a, and C5aR1 inhibitor (PMX53) reduced tumor growth and angiogenesis in ovarian cancer[14]. PMX205 showed anti-cancer activity and increased effectiveness in RT for intestinal cancer[18]. Collectively, inhibitors of the C5a-C5aR1 axis (PMX53, PMX205) have shown promising anti-cancer efficiency and protection of normal tissue. These reports led us to test cognitive function in our WT murine brain cancer and cranial RT models to determine if C5aR1 inhibitor treatment alleviated RT-induced normal tissue toxicity. In our study, GBM or astrocytoma tumor burden itself reduced cognitive function compared to unirradiated cancer-free controls (**Fig. 4F**). Cranial RT to either GBM- or astrocytoma-bearing mice also impaired cognitive function. Importantly, PMX205 treatment to either cancer-bearing or cancer-bearing mice +RT significantly ameliorated RICD. This is a significant result, and it reinforces findings from the cancer-free irradiated mice (**Fig. 1**), which validate the neuroprotective effect of PMX205 on cognitive function.

Our study demonstrates that targeting C5aR1 in the irradiated brain will not disrupt the beneficial effects of the upstream complement components but will prevent microglial activation and astrogliosis and, importantly, protect from cranial RT-induced normal tissue toxicity and RICD in cancer-free and cancer-bearing brains. C5aR1 inhibitors have shown protective effects in many neurodegenerative and inflammatory disease models, including asthma, sepsis, ischemia, Huntington's disease, ALS, and TBI[43-48]. Human clinical trials on C5aR1 inhibitors (PMX53, CCX168) for rheumatoid arthritis and ANCA-associated vasculitis showed excellent safety profiles and lack of toxicity[13,49], and Tavenos (CCX168) is now FDA-approved for the autoimmune disease. These pre-clinical mouse and human clinical trial data suggest that inhibition of the C5a-C5aR1 signaling axis is not harmful, emphasizing our approach's translational feasibility to improve the QOL for millions of cancer survivors.

## LIMITATIONS OF THE STUDY

We provide proof of the principle that C5a-C5aR1 axis inhibition via either genetic ablation of C5aR1 or pharmacologic inhibition using PMX205 reverses the detrimental neuroinflammatory and neurocognitive consequences of cranial RT. We showed this using pre-clinical cancer-free and brain cancer-bearing mouse models. Cranial RT in the clinic is often scheduled as a fractionated or hypofractionated dosing regimen, which includes multiple radiation exposures. Thus, the translational feasibility of PMX205 should also be tested using a fractionated cranial RT paradigm to approximate the biological effective dose (B.E.D.) regime for late RICD. A fractionated RT regime is expected to eliminate brain cancer and allow the study of cellular and molecular endpoints of microglial, astrocytic, and synaptic function *in vivo*. A longitudinal cognitive function assessment before and post-RT and after completion of C5aR1 inhibitor treatment would allow the restoration of cognitive function in the injured brain to be studied. Albeit, such cognitive testing may lead to fatigue in animals and limit testing of invasive tasks. Nonetheless, these proposed experiments will determine the long-term safety and neuroprotective efficacy of C5aR1 inhibitors for cranial RT-induced normal tissue toxicity.

**ACKNOWLDEGMENTS**

This work was supported by the National Institute of Health (NIH) awards (R01CA251110, R01CA262213, and R01CA276212), American Brain Tumor Association Discovery award (DG2000029), HESI-Thrive award (Health and Environmental Sciences Institute, 2021), and the University of California Irvine (UCI) Chao Family Comprehensive Cancer Center (CFCCC) Pilot award to M.M.A. We also thank the support of the UCI CFCCC Biostatitics shared resource supported by the National Cancer Institute (NIH, award P30CA062203). The content is solely the responsibility of the authors and does not necessarily represent the official views of the NIH.

**AUTHOR CONTRIBUTIONS**

Conception and design: MMA, AJT, JEB

Development of methodology: RPK, AHD, SMK, LA, MM, ARV, MTU, SM

Acquisition of data: RPK, AHD, SMK, LA, MM, ARV, MTU, SM

Analysis and interpretation of data: RPK, AHD, SMK, JEB, MMA

Writing, review and/or revision of the manuscript: RPK, AHD, MMA, AJT, JEB

Administrative, technical, or material support: RJC, TMW, AJT, JEB, MMA.

Study supervision: RPK, JEB, MMA.

## REFERENCES


1. Dietrich, J., Gondi, V., and Mehta, M. (2023). Delayed complications of cranial irradiation. Available on: https://www.uptodate.com/contents/delayed-complications-of-cranial-irradiation?csi=c79760e5-e373-463b-b181-3eefa0769caa&source=contentShare. UpToDate, https://www.uptodate.com/contents/delayed-complications-of-cranial-irradiation?csi=c79760e5-e373-463b-b181-3eefa0769caa&source=contentShare.
2. Lawrence, D.R., van den Bent, M., and Shih, H.A. (2023). Treatment and prognosis of diffuse (grade II) and anaplastic (grade III) astrocytomas in adults. https://www.uptodate.com/contents/treatment-and-prognosis-of-idh-mutant-astrocytomas-in-adults. https://www.uptodate.com/contents/treatment-and-prognosis-of-diffuse-grade-ii-and-anaplastic-grade-iii-astrocytomas-in-adults.
3. Markarian, M., Krattli, R.P., Jr., Baddour, J.D., Alikhani, L., Giedzinski, E., Usmani, M.T., Agrawal, A., Baulch, J.E., Tenner, A.J., and Acharya, M.M. (2021). Glia-Selective Deletion of Complement C1q Prevents Radiation-Induced Cognitive Deficits and Neuroinflammation. Cancer Res *81*, 1732-1744. 10.1158/0008-5472.CAN-20-2565.
4. Greene-Schloesser, D., Moore, E., and Robbins, M.E. (2013). Molecular pathways: radiation-induced cognitive impairment. Clinical cancer research : an official journal of the American Association for Cancer Research *19*, 2294-2300. 10.1158/1078-0432.CCR-11-2903.
5. Coulthard, L.G., Hawksworth, O.A., and Woodruff, T.M. (2018). Complement: The Emerging Architect of the Developing Brain. Trends Neurosci *41*, 373-384. 10.1016/j.tins.2018.03.009.
6. Gomez-Arboledas, A., Acharya, M.M., and Tenner, A.J. (2021). The Role of Complement in Synaptic Pruning and Neurodegeneration. Immunotargets Ther *10*, 373-386. 10.2147/ITT.S305420.
7. Hernandez, M.X., Jiang, S., Cole, T.A., Chu, S.H., Fonseca, M.I., Fang, M.J., Hohsfield, L.A., Torres, M.D., Green, K.N., Wetsel, R.A., et al. (2017). Prevention of C5aR1 signaling delays microglial inflammatory polarization, favors clearance pathways and suppresses cognitive loss. Mol Neurodegener *12*, 66. 10.1186/s13024-017-0210-z.
8. Fonseca, M.I., Ager, R.R., Chu, S.H., Yazan, O., Sanderson, S.D., LaFerla, F.M., Taylor, S.M., Woodruff, T.M., and Tenner, A.J. (2009). Treatment with a C5aR antagonist decreases pathology and enhances behavioral performance in murine models of Alzheimer's disease. Journal of immunology *183*, 1375-1383. 10.4049/jimmunol.0901005.
9. Gomez-Arboledas, A., Carvalho, K., Balderrama-Gutierrez, G., Chu, S.H., Liang, H.Y., Schartz, N.D., Selvan, P., Petrisko, T.J., Pan, M.A., Mortazavi, A., and Tenner, A.J. (2022). C5aR1 antagonism alters microglial polarization and mitigates disease progression in a mouse model of Alzheimer's disease. Acta Neuropathol Commun *10*, 116. 10.1186/s40478-022-01416-6.
10. Carvalho, K., Schartz, N.D., Balderrama-Gutierrez, G., Liang, H.Y., Chu, S.H., Selvan, P., Gomez-Arboledas, A., Petrisko, T.J., Fonseca, M.I., Mortazavi, A., and Tenner, A.J. (2022). Modulation of C5a-C5aR1 signaling alters the dynamics of AD progression. Journal of neuroinflammation *19*, 178. 10.1186/s12974-022-02539-2.
11. Kumar, V., Lee, J.D., Clark, R.J., Noakes, P.G., Taylor, S.M., and Woodruff, T.M. (2020). Preclinical Pharmacokinetics of Complement C5a Receptor Antagonists PMX53 and PMX205 in Mice. ACS Omega *5*, 2345-2354. 10.1021/acsomega.9b03735.
12. Schartz, N.D., Liang, H.Y., Carvalho, K., Chu, S.H., Mendoza-Arvilla, A., Petrisko, T.J., Gomez-Arboledas, A., Mortazavi, A., and Tenner, A.J. (2023). C5aR1 antagonism suppresses inflammatory glial gene expression and alters cellular signaling in an aggressive Alzheimer's model. bioRxiv. 10.1101/2023.08.22.554306.

13. Jayne, D.R.W., Merkel, P.A., Schall, T.J., Bekker, P., and Group, A.S. (2021). Avacopan for the Treatment of ANCA-Associated Vasculitis. N Engl J Med *384*, 599-609. 10.1056/NEJMoa2023386.
14. Nunez-Cruz, S., Gimotty, P.A., Guerra, M.W., Connolly, D.C., Wu, Y.Q., DeAngelis, R.A., Lambris, J.D., Coukos, G., and Scholler, N. (2012). Genetic and pharmacologic inhibition of complement impairs endothelial cell function and ablates ovarian cancer neovascularization. Neoplasia *14*, 994-1004. 10.1593/neo.121262.
15. Markiewski, M.M., DeAngelis, R.A., Benencia, F., Ricklin-Lichtsteiner, S.K., Koutoulaki, A., Gerard, C., Coukos, G., and Lambris, J.D. (2008). Modulation of the antitumor immune response by complement. Nature immunology *9*, 1225-1235. 10.1038/ni.1655.
16. Zhang, X., Kimura, Y., Fang, C., Zhou, L., Sfyroera, G., Lambris, J.D., Wetsel, R.A., Miwa, T., and Song, W.C. (2007). Regulation of Toll-like receptor-mediated inflammatory response by complement in vivo. Blood *110*, 228-236. 10.1182/blood-2006-12-063636.
17. Bouwens van der Vlis, T.A.M., Kros, J.M., Mustafa, D.A.M., van Wijck, R.T.A., Ackermans, L., van Hagen, P.M., and van der Spek, P.J. (2018). The complement system in glioblastoma multiforme. Acta Neuropathol Commun *6*, 91. 10.1186/s40478-018-0591-4.
18. Olcina, M.M., Melemenidis, S., Nambiar, D.K., Kim, R.K., Casey, K.M., von Eyben, R., Woodruff, T.M., Graves, E.G., Le, Q.-T., Stucki, M., and Giaccia, A.J. (2020). Targeting C5aR1 Increases the Therapeutic Window of Radiotherapy. bioRxiv, 2020.2010.2027.358036. 10.1101/2020.10.27.358036.
19. Hollmann, T.J., Mueller-Ortiz, S.L., Braun, M.C., and Wetsel, R.A. (2008). Disruption of the C5a receptor gene increases resistance to acute Gram-negative bacteremia and endotoxic shock: opposing roles of C3a and C5a. Mol Immunol *45*, 1907-1915. 10.1016/j.molimm.2007.10.037.
20. Milad, M.R., and Quirk, G.J. (2012). Fear extinction as a model for translational neuroscience: ten years of progress. Annual review of psychology *63*, 129-151. 10.1146/annurev.psych.121208.131631.
21. Schubert, I., Ahlbrand, R., Winter, A., Vollmer, L., Lewkowich, I., and Sah, R. (2018). Enhanced fear and altered neuronal activation in forebrain limbic regions of CX3CR1-deficient mice. Brain Behav Immun *68*, 34-43. 10.1016/j.bbi.2017.09.013.
22. Parihar, V.K., Pasha, J., Tran, K.K., Craver, B.M., Acharya, M.M., and Limoli, C.L. (2014). Persistent changes in neuronal structure and synaptic plasticity caused by proton irradiation. Brain structure & function. 10.1007/s00429-014-0709-9.
23. Parihar, V.K., Allen, B.D., Caressi, C., Kwok, S., Chu, E., Tran, K.K., Chmielewski, N.N., Giedzinski, E., Acharya, M.M., Britten, R.A., et al. (2016). Cosmic radiation exposure and persistent cognitive dysfunction. Scientific reports *6*, 34774. 10.1038/srep34774.
24. Makale, M.T., McDonald, C.R., Hattangadi-Gluth, J.A., and Kesari, S. (2017). Mechanisms of radiotherapy-associated cognitive disability in patients with brain tumours. Nature reviews. Neurology *13*, 52-64. 10.1038/nrneurol.2016.185.
25. Gomez-Arboledas, A., Fonseca, M.I., Kramar, E., Chu, S.H., Schartz, N., Selvan, P., Wood, M.A., and Tenner, A.J. (2023). C5aR1 signaling promotes region and age dependent synaptic pruning in models of Alzheimer's Disease. bioRxiv. 10.1101/2023.09.29.560234.
26. Acharya, M.M., Green, K.N., Allen, B.D., Najafi, A.R., Syage, A., Minasyan, H., Le, M.T., Kawashita, T., Giedzinski, E., Parihar, V.K., et al. (2016). Elimination of microglia improves cognitive function following cranial irradiation. Scientific reports *6*, 31545. 10.1038/srep31545.
27. Acharya, M.M., Christie, L.A., Lan, M.L., Giedzinski, E., Fike, J.R., Rosi, S., and Limoli, C.L. (2011). Human neural stem cell transplantation ameliorates radiation-induced cognitive dysfunction. Cancer Res *71*, 4834-4845. 10.1158/0008-5472.CAN-11-0027.
28. Montay-Gruel, P., Acharya, M.M., Petersson, K., Alikhani, L., Yakkala, C., Allen, B.D., Ollivier, J., Petit, B., Jorge, P.G., Syage, A.R., et al. (2019). Long-term neurocognitive benefits of FLASH

radiotherapy driven by reduced reactive oxygen species. Proc Natl Acad Sci U S A *116*, 10943-10951. 10.1073/pnas.1901777116.

29. Acharya, M.M., Baulch, J.E., Lusardi, T., Allen, B.D., Chmielewski, N.N., Baddour, A.A.D., Limoli, C.L., and Boison, D. (2016). Adenosine Kinase Inhibition Protects against Cranial Radiation-Induced Cognitive Dysfunction. Frontiers in molecular neuroscience *9*, 1-10. 10.3389/fnmol.2016.00042.
30. Acharya, M.M., Baulch, J.E., Lusardi, T.A., Allen, B.D., Chmielewski, N.N., Baddour, A.A., Limoli, C.L., and Boison, D. (2016). Adenosine Kinase Inhibition Protects against Cranial Radiation-Induced Cognitive Dysfunction. Frontiers in molecular neuroscience *9*, 42. 10.3389/fnmol.2016.00042.
31. Acharya, M.M., Martirosian, V., Christie, L.A., and Limoli, C.L. (2014). Long-term cognitive effects of human stem cell transplantation in the irradiated brain. International journal of radiation biology *90*, 816-820. 10.3109/09553002.2014.927934.
32. Hinkle, J.J., Olschowka, J.A., Williams, J.P., and O'Banion, M.K. (2023). Pharmacologic Manipulation of Complement Receptor 3 Prevents Dendritic Spine Loss and Cognitive Impairment After Acute Cranial Radiation. Int J Radiat Oncol Biol Phys. 10.1016/j.ijrobp.2023.12.017.
33. Woods, G.F., Oh, W.C., Boudewyn, L.C., Mikula, S.K., and Zito, K. (2011). Loss of PSD-95 enrichment is not a prerequisite for spine retraction. J Neurosci *31*, 12129-12138. 10.1523/JNEUROSCI.6662-10.2011.
34. Levy, A.M., Gomez-Puertas, P., and Tumer, Z. (2022). Neurodevelopmental Disorders Associated with PSD-95 and Its Interaction Partners. International journal of molecular sciences *23*. 10.3390/ijms23084390.
35. Chugh, D., Nilsson, P., Afjei, S.A., Bakochi, A., and Ekdahl, C.T. (2013). Brain inflammation induces post-synaptic changes during early synapse formation in adult-born hippocampal neurons. Exp Neurol *250*, 176-188. 10.1016/j.expneurol.2013.09.005.
36. Levinson, J.N., Chery, N., Huang, K., Wong, T.P., Gerrow, K., Kang, R., Prange, O., Wang, Y.T., and El-Husseini, A. (2005). Neuroligins mediate excitatory and inhibitory synapse formation: involvement of PSD-95 and neurexin-1beta in neuroligin-induced synaptic specificity. J Biol Chem *280*, 17312-17319. 10.1074/jbc.M413812200.
37. Urbanska, M., Swiech, L., and Jaworski, J. (2012). Developmental plasticity of the dendritic compartment: focus on the cytoskeleton. Advances in experimental medicine and biology *970*, 265-284. 10.1007/978-3-7091-0932-8_12.
38. Parihar, V.K., and Limoli, C.L. (2013). Cranial irradiation compromises neuronal architecture in the hippocampus. Proc Natl Acad Sci U S A *110*, 12822-12827. 10.1073/pnas.1307301110.
39. Hernandez, M.X., Namiranian, P., Nguyen, E., Fonseca, M.I., and Tenner, A.J. (2017). C5a Increases the Injury to Primary Neurons Elicited by Fibrillar Amyloid Beta. ASN Neuro *9*, 1759091416687871. 10.1177/1759091416687871.
40. Bouwens, T.A., Trouw, L.A., Veerhuis, R., Dirven, C.M., Lamfers, M.L., and Al-Khawaja, H. (2015). Complement activation in Glioblastoma multiforme pathophysiology: evidence from serum levels and presence of complement activation products in tumor tissue. Journal of neuroimmunology *278*, 271-276. 10.1016/j.jneuroim.2014.11.016.
41. Gasque, P., Thomas, A., Fontaine, M., and Morgan, B.P. (1996). Complement activation on human neuroblastoma cell lines in vitro: route of activation and expression of functional complement regulatory proteins. Journal of neuroimmunology *66*, 29-40. 10.1016/0165-5728(96)00015-x.
42. Zhu, H., Yu, X., Zhang, S., and Shu, K. (2021). Targeting the Complement Pathway in Malignant Glioma Microenvironments. Front Cell Dev Biol *9*, 657472. 10.3389/fcell.2021.657472.
43. Woodruff, T.M., Nandakumar, K.S., and Tedesco, F. (2011). Inhibiting the C5-C5a receptor axis. Mol Immunol *48*, 1631-1642. 10.1016/j.molimm.2011.04.014.

44. Woodruff, T.M., Costantini, K.J., Crane, J.W., Atkin, J.D., Monk, P.N., Taylor, S.M., and Noakes, P.G. (2008). The complement factor C5a contributes to pathology in a rat model of amyotrophic lateral sclerosis. Journal of immunology *181*, 8727-8734.
45. Woodruff, T.M., Crane, J.W., Proctor, L.M., Buller, K.M., Shek, A.B., de Vos, K., Pollitt, S., Williams, H.M., Shiels, I.A., Monk, P.N., and Taylor, S.M. (2006). Therapeutic activity of C5a receptor antagonists in a rat model of neurodegeneration. FASEB J *20*, 1407-1417. 10.1096/fj.05-5814com.
46. Woodruff, T.M., Pollitt, S., Proctor, L.M., Stocks, S.Z., Manthey, H.D., Williams, H.M., Mahadevan, I.B., Shiels, I.A., and Taylor, S.M. (2005). Increased potency of a novel complement factor 5a receptor antagonist in a rat model of inflammatory bowel disease. The Journal of pharmacology and experimental therapeutics *314*, 811-817. 10.1124/jpet.105.086835.
47. Sewell, D.L., Nacewicz, B., Liu, F., Macvilay, S., Erdei, A., Lambris, J.D., Sandor, M., and Fabry, Z. (2004). Complement C3 and C5 play critical roles in traumatic brain cryoinjury: blocking effects on neutrophil extravasation by C5a receptor antagonist. Journal of neuroimmunology *155*, 55-63. 10.1016/j.jneuroim.2004.06.003.
48. Holland, M.C., Morikis, D., and Lambris, J.D. (2004). Synthetic small-molecule complement inhibitors. Curr Opin Investig Drugs *5*, 1164-1173.
49. Vergunst, C.E., Gerlag, D.M., Dinant, H., Schulz, L., Vinkenoog, M., Smeets, T.J., Sanders, M.E., Reedquist, K.A., and Tak, P.P. (2007). Blocking the receptor for C5a in patients with rheumatoid arthritis does not reduce synovial inflammation. Rheumatology (Oxford) *46*, 1773-1778. 10.1093/rheumatology/kem222.

**Figure 1.**

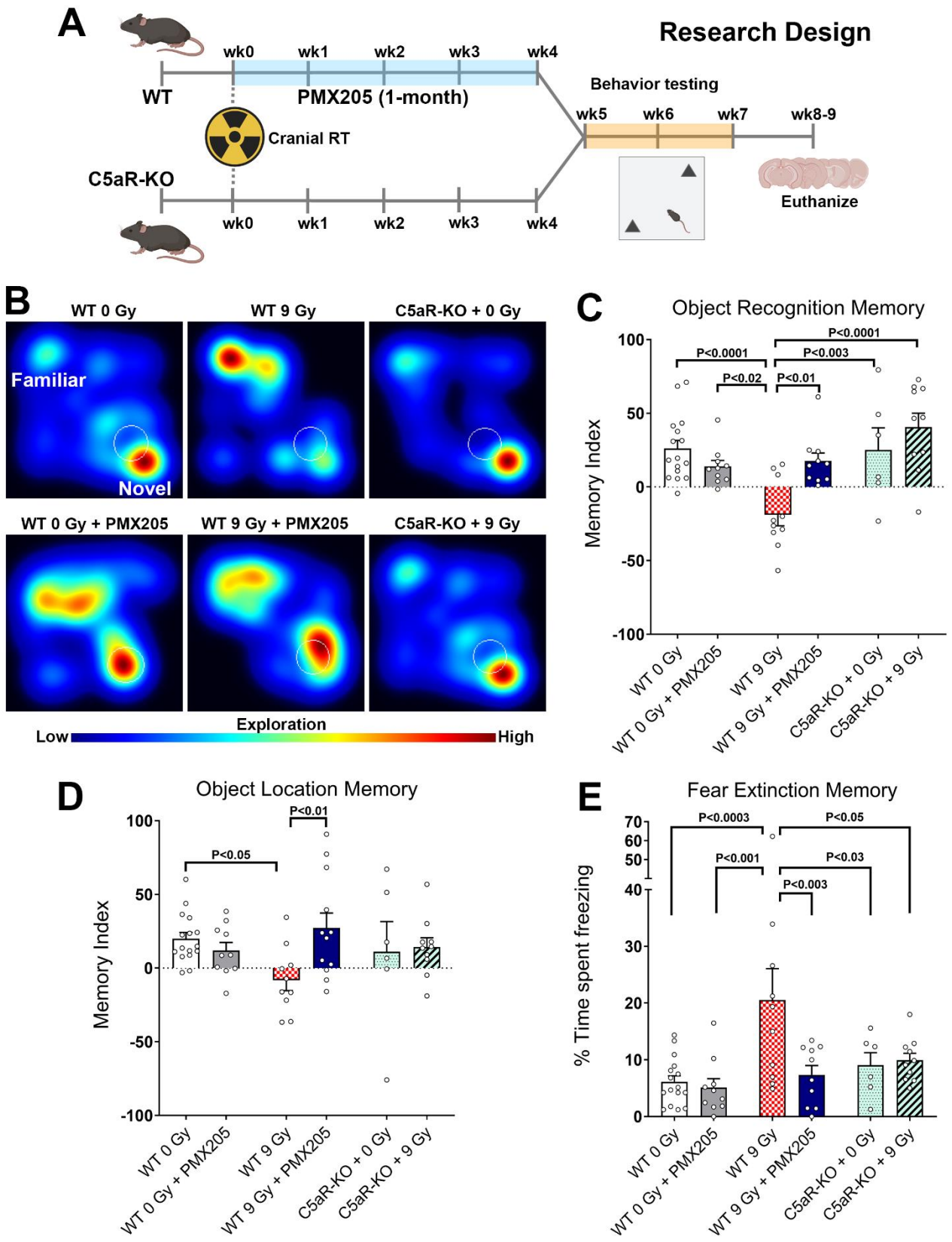
A
Research Design
wk0
wk1
wk2
wk3
wk4
WT
PMX205 (1-month)
Cranial RT
C5aR-KO
Behavior testing
wk5
wk6
wk7
wk8-9
Euthanize
B
WT 0 Gy
WT 9 Gy
C5aR-KO + 0 Gy
Familiar
Novel
WT 0 Gy + PMX205
WT 9 Gy + PMX205
C5aR-KO + 9 Gy
Low
Exploration
High
C
Object Recognition Memory
Memory Index
P<0.0001
P<0.02
P<0.01
P<0.003
P<0.0001
WT 0 Gy
WT 0 Gy + PMX205
WT 9 Gy
WT 9 Gy + PMX205
C5aR-KO + 0 Gy
C5aR-KO + 9 Gy
D
Object Location Memory
Memory Index
P<0.05
P<0.01
E
Fear Extinction Memory
% Time spent freezing
P<0.0003
P<0.05
P<0.001
P<0.03
P<0.003

**FIGURE 1. C5aR1 knockout or inhibition prevents cranial radiation-induced cognitive impairments.**

**(A)** Research design: Four-month-old C57Bl6 WT and C5aR1-KO mice received 0 or 9 Gy cranial radiotherapy (CRT). At 48h post-CRT, WT mice received PMX205 treatment (1 mg/kg SQ for the first week in addition to 20 µg/ml, or 100 µg per day in drinking water for 1-month). All mice were administered cognitive function tasks (Object Recognition Memory, ORM; Object Location Memory, OLM; and fear extinction memory consolidation, FE) 1-month later and euthanized for tissue collection.

**(B)** Representative heat maps depicting mice exploring novel or familiar objects during the ORM task. Irradiated WT mice (WT 9 Gy) did not show a preference for novel objects.

**(C)** The tendency to explore novel objects (ORM) was derived from the Memory Index: ([Novel object exploration time/Total exploration time] – [Familiar object exploration time/Total exploration time]) ×100. WT 9 Gy mice showed significantly impaired cognitive function, as indicated by the reduced preference towards the novel object compared to the WT 0 Gy, WT 0 Gy+PMX205, C5aR1-KO+0 Gy, and C5aR1-KO+9 Gy groups. Importantly, irradiated C5aR1-KO mice and WT 9 Gy+PMX205 did not show a decline in the memory index.

**(D)** Irradiated WT mice spent significantly less time exploring the novel object locations during the OLM task. WT 9 Gy mice +PMX205 showed significantly improved memory index compared to WT 9 Gy mice +Vehicle. Irradiated C5aR1-KO mice showed a trend of spatial exploration improvements (a positive Memory Index) during the OLM task.

**(E)** C5aR1 inhibition or KO significantly improved fear memory consolidation (FE test). WT+0 Gy and WT 0 Gy+PMX205 showed abolished fear memory (reduced freezing, intact memory consolidation) compared with WT 9 Gy mice. Importantly, WT 9 Gy mice +PMX205 and C5aR1-KO+0 Gy and 9 Gy mice successfully abolished fear memory (reduced freezing) compared to the WT 9 Gy group. Mean±SEM (*N*=8-16 mice per group).

**Figure 2.**

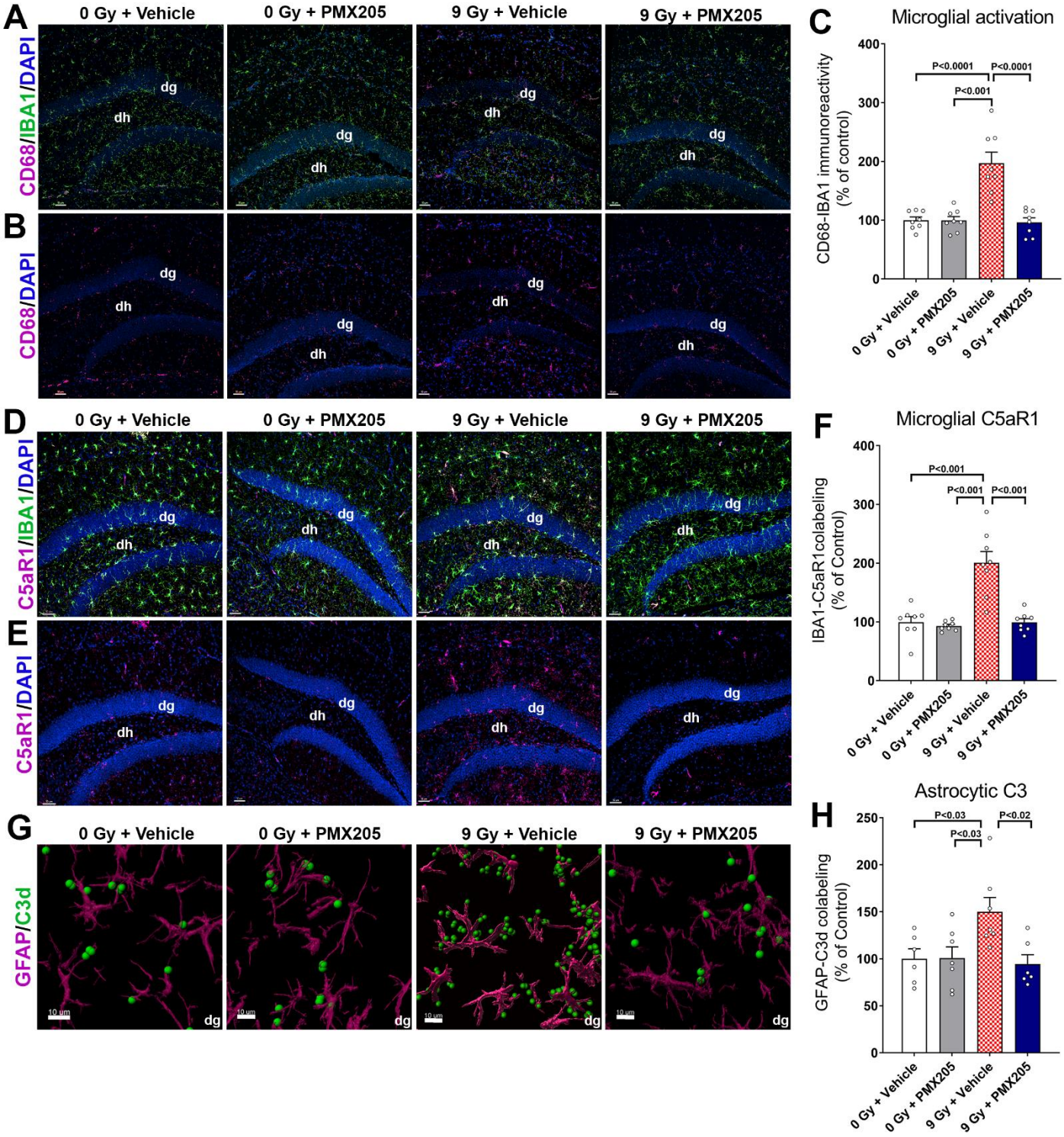
A
0 Gy + Vehicle
0 Gy + PMX205
9 Gy + Vehicle
9 Gy + PMX205
CD68/IBA1/DAPI
dg
dh
B
CD68/DAPI
C
Microglial activation
CD68-IBA1 immunoreactivity (% of control)
P<0.0001
P<0.0001
P<0.001
D
C5aR1/IBA1/DAPI
E
C5aR1/DAPI
F
Microglial C5aR1
IBA1-C5aR1colabeling (% of Control)
P<0.001
P<0.001
P<0.001
G
GFAP/C3d
10 µm
H
Astrocytic C3
GFAP-C3d colabeling (% of Control)
P<0.03
P<0.03
P<0.02

**FIGURE 2. C5aR inhibition prevents radiation-induced neuroinflammation.**

**(A)** Dual immunofluorescence staining, confocal microscopy, and 3D algorithm-based, volumetric quantification for the microglial activation (CD68-IBA1 immunoreactivity, magenta-green) in the WT mice show cranial irradiation (9 Gy + Vehicle)-induced elevated CD68 expression by the $IBA1^+$ microglia in the hippocampus (*dh*, dentate hilus; *dg*, dentate gyrus) compared to 0 Gy+Vehicle. **(B)** A separate CD68-DAPI channel (magenta-blue) is shown for each group. **(C)** C5aR inhibition (PMX205) in WT mice did not elevate CD68 immunoreactivity in the irradiated brain (9 Gy+PMX205), indicating prevention of inflammation.

**(D-E)** Volumetric quantification for the microglial C5aR1 expression (C5aR1-IBA1 immunoreactivity, magenta-green) showed a radiation-induced increase in the microglial-C5aR1 in the WT hippocampal *dg* and *dh* compared to unirradiated controls. PMX205 treatment reduced microglial-C5aR1 expression compared to the 9 Gy mice +vehicle (**F**).

**(G)** Analysis of astrogliosis (GFAP-C3d) showed radiation-induced elevation in $GFAP^+$ astrocytic surface co-labeled with complement C3d (GFAP surface rendering, magenta, and C3d spot rendering, green) in the 9 Gy+Vehicle compared to 0 Gy+Vehicle or 0 Gy+PMX205 groups in the hippocampal *dg*. 9 Gy mice receiving C5aR inhibitor (PMX205) did not show elevated GFAP-C3d immunoreactivity, indicating reduced astrogliosis **(H)**. Mean±SEM (*N*=6-8 per group). Scale bars, 50 µm (**A-B, D-E**) and 10 µm (**G**).

**Figure 3.**

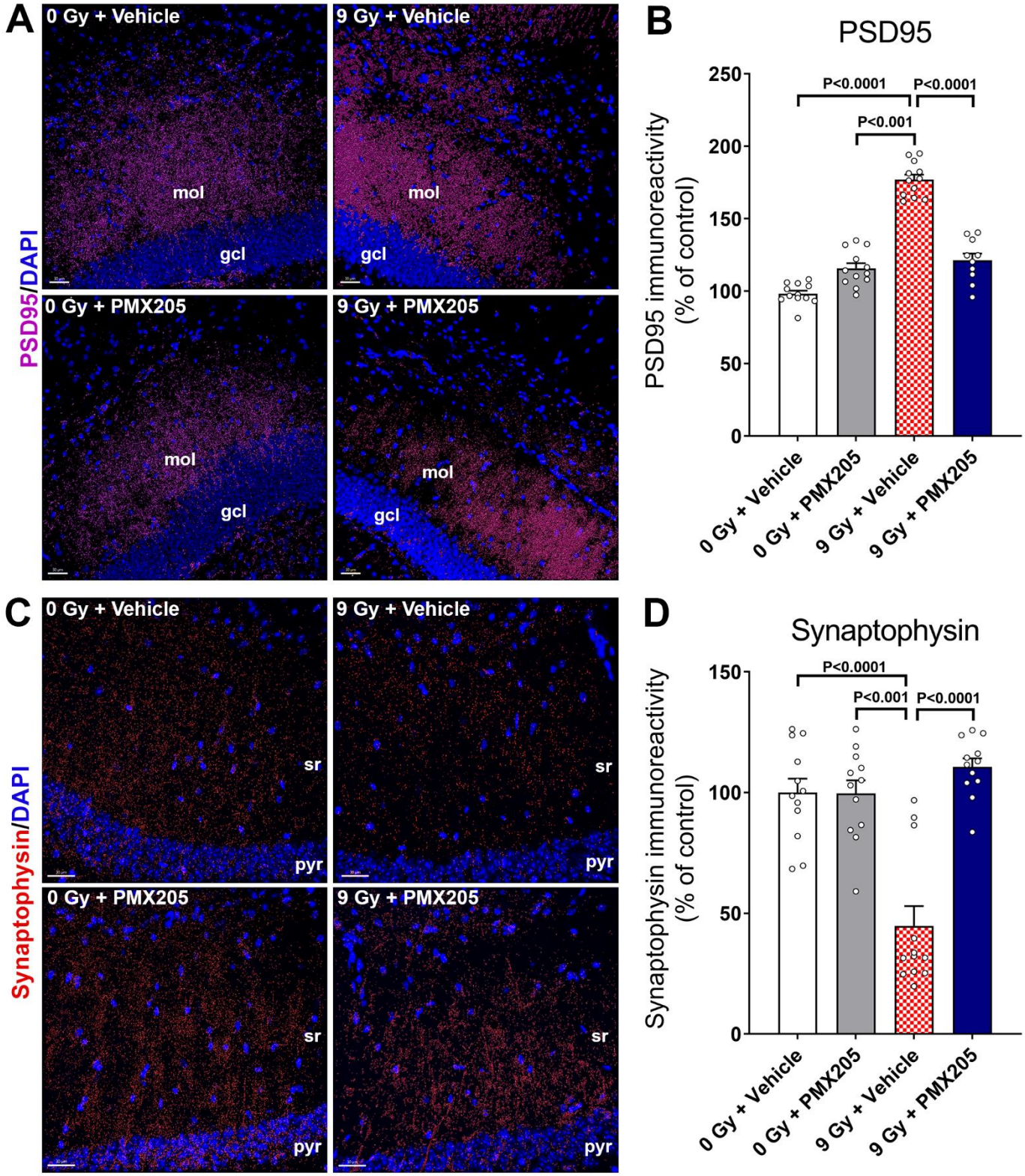
A
0 Gy + Vehicle
9 Gy + Vehicle
0 Gy + PMX205
9 Gy + PMX205
mol
gcl
PSD95/DAPI
B
PSD95
PSD95 immunoreactivity (% of control)
P<0.0001
P<0.0001
P<0.001
0 Gy + Vehicle
0 Gy + PMX205
9 Gy + Vehicle
9 Gy + PMX205
C
sr
pyr
Synaptophysin/DAPI
D
Synaptophysin
Synaptophysin immunoreactivity (% of control)
P<0.0001
P<0.001
P<0.0001

**FIGURE 3. C5aR antagonism prevents radiation-induced loss of synaptic integrity.**

**(A-B)** Immunofluorescence staining, confocal microscopy, and 3D algorithm-based quantification for the post-synaptic density protein, PSD95 (magenta, DAPI nuclear counter stain) in the hippocampus showed significantly elevated PSD95 in 9 Gy+Vehicle compared to 0 Gy+Vehicle group. Irradiated mice receiving a C5aR antagonist did not show an aberrant PSD95 elevation (9 Gy+PMX205).

**(C-D)** In contrast, volumetric quantification of hippocampal synaptic vesicle protein synaptophysin (red, DAPI nuclear counter stain) showed a significant decline post-RT (9 Gy+Vehicle) compared to 0 Gy+Vehicle group. PMX205 treatment in the irradiated mice prevented loss of synaptophysin, indicating the neuroprotective impact of C5aR inhibition against irradiation. Mean ± SEM (*N*=8-10 mice per group). Scale bars, 30 µm (**A, C**).

**Figure 4.**

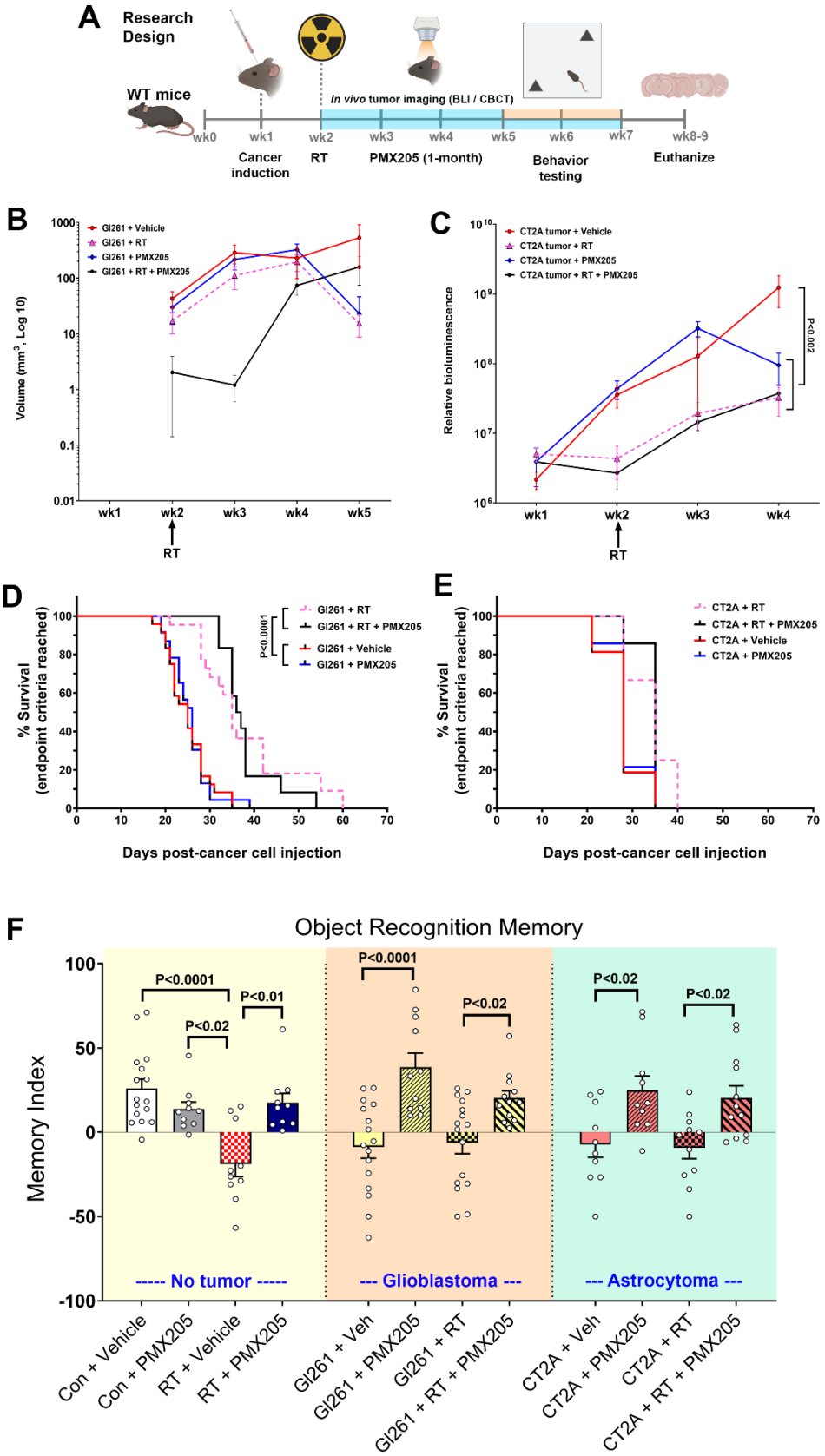
A
Research Design
WT mice
In vivo tumor imaging (BLI / CBCT)
wk0
wk1
wk2
wk3
wk4
wk5
wk6
wk7
wk8-9
Cancer induction
RT
PMX205 (1-month)
Behavior testing
Euthanize
B
Gl261 + Vehicle
Gl261 + RT
Gl261 + PMX205
Gl261 + RT + PMX205
Volume (mm3, Log 10)
RT
C
CT2A tumor + Vehicle
CT2A tumor + RT
CT2A tumor + PMX205
CT2A tumor + RT + PMX205
Relative bioluminescence
P<0.002
RT
D
% Survival (endpoint criteria reached)
P<0.0001
Gl261 + RT
Gl261 + RT + PMX205
Gl261 + Vehicle
Gl261 + PMX205
Days post-cancer cell injection
E
CT2A + RT
CT2A + RT + PMX205
CT2A + Vehicle
CT2A + PMX205
% Survival (endpoint criteria reached)
Days post-cancer cell injection
F
Object Recognition Memory
Memory Index
P<0.0001
P<0.02
P<0.01
P<0.0001
P<0.02
P<0.02
P<0.02
----- No tumor -----
--- Glioblastoma ---
--- Astrocytoma ---
Con + Vehicle
Con + PMX205
RT + Vehicle
RT + PMX205
Gl261 + Veh
Gl261 + PMX205
Gl261 + RT
Gl261 + RT + PMX205
CT2A + Veh
CT2A + PMX205
CT2A + RT
CT2A + RT + PMX205

**FIGURE 4. C5aR inhibition in the astrocytoma- and glioblastoma-bearing mice reversed cranial radiation-induced cognitive decline without interfering with tumor growth or survival.**

**(A)** Schematic representation of research design. C57Bl6 mice received orthotopic implantation of cancer cells (Gl261 glioblastoma, CT2A-luc astrocytoma) in the caudate putamen. A cohort of brain cancer-bearing mice received cranial radiotherapy (RT) 1-week post-tumor induction. Mice were divided into the following groups (2 tumor types): Tumor+Vehicle, Tumor+RT, Tumor+PMX205, and Tumor+RT+PMX205. At 48h post-RT, mice received PMX205 treatment (1 mg/kg SQ for the first week in addition to 20 µg/ml, or 100 µg per day in drinking water for 1-month). Tumor growth and progression were monitored weekly by *in vivo* tumor imaging. Bioluminescence Imaging (BLI) was used for CT2A-luc$^+$ astrocytoma, and iodine contrast, Cone-Beam Computerized Tomography (CBCT) scanning was used for the detection and volumetric measurement of Gl261$^+$ glioblastoma. At 3-4-weeks post-RT, mice were administered object recognition memory task (ORM) and euthanized for tissue collection.

**(B)** CBCT-acquired Gl261+ glioblastoma showed a steady progression through one week post-implantation and RT. At the end of the study, no significant impact of C5aR1 inhibition or RT on the tumor volume was found.

**(C)** The CT2A-luc$^+$ astrocytoma showed rapid growth 1-week post-implantation. C5aR1 inhibition and RT (CT2A+PMX205, CT2A+RT, and CT2A+RT+PMX205) showed a significant reduction in tumor volume compared to the CT2A+vehicle group at the end of the study.

**(D-E)** Kaplan-Meier survival estimates showed improved survival of Gl261$^+$ glioblastoma-bearing mice receiving RT or RT+PMX205 treatments compared to Vehicle or PMX205 treatment alone. CT2A$^+$ astrocytoma showed comparable survival estimates for all groups of mice.

**(F)** At 3-4 weeks post-RT, cognitive function assessment (ORM task) was performed. To compare cognitive function, intact (no tumor) WT mice performance (as in Fig. 1C) is plotted along with glioblastoma and astrocytoma groups. 9 Gy cranial RT significantly reduced memory index (RT+Vehicle) in mice without tumors. Tumor burden itself (Gl261+Veh and CT2A+Veh) and tumor-bearing mice receiving RT (Gl261+RT and CT2A+RT) showed a significant reduction in the ORM task performance (reduced Memory Index). In contrast, tumor-bearing mice ±RT receiving C5aR1 inhibitor treatment showed significant improvements in Memory Indices (Gl261+PMX205,

Gl261+RT+PMX205, CT2A+PMX205, and CT2A+RT+PMX205), indicating neuroprotective impact of C5aR inhibition. Mean±SEM (*N*=12-24 mice per group).

## SUPPLEMENTAL INFORMATION

Krattli *et al.*, Complement C5a receptor 1 blockade reverses cognitive deficits following cranial radiation therapy for brain cancer

### Supplemental Figure S1

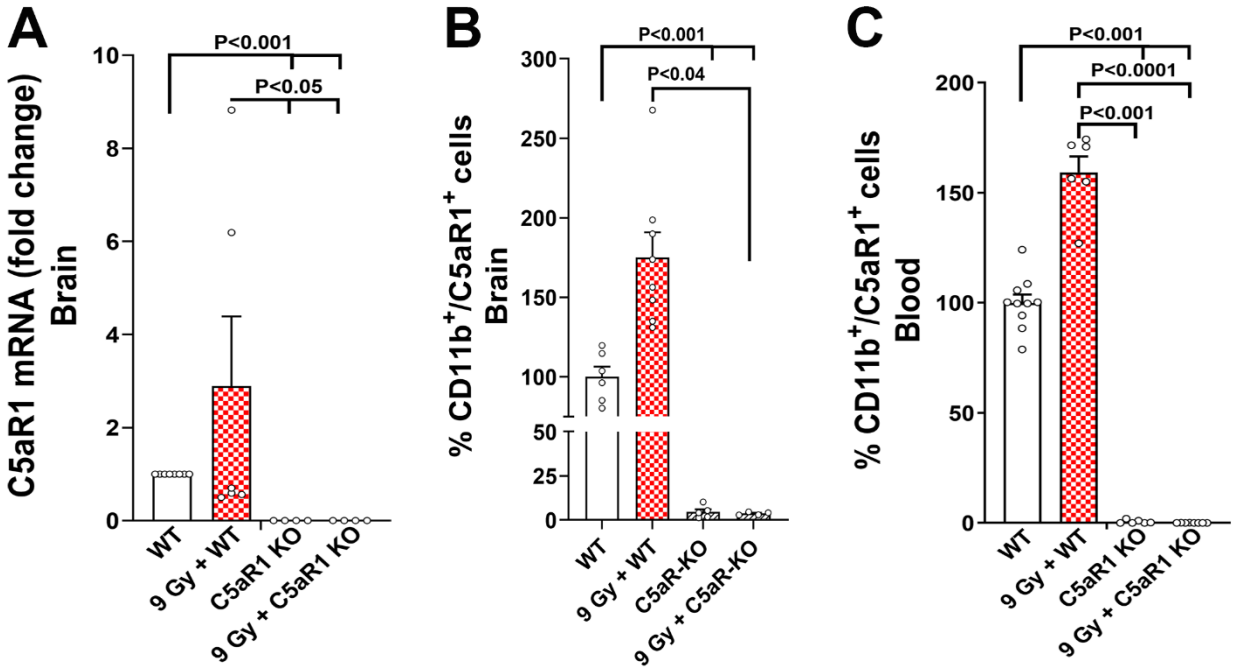


**Supplemental Figure S1:** Characterization of C5aR1 expression in the WT and C5aR1 KO mice brains (**A-B**) and blood (**B**). (**A**) qPCR for C5aR1 mRNA expression showed nearly complete ablation of C5aR1 transcript in the 0 Gy and 9 Gy irradiated brains of C5aR1 KO mice. **(B-C)** Flow cytometry analysis of C5aR1 from brains and blood also showed nearly complete ablation of C5aR1 *in vivo*. Mean ± SEM (*N*=6-10 mice per group). *P* values were derived from two-way ANOVA and Bonferroni's post hoc test.

**Supplemental Figure S2**

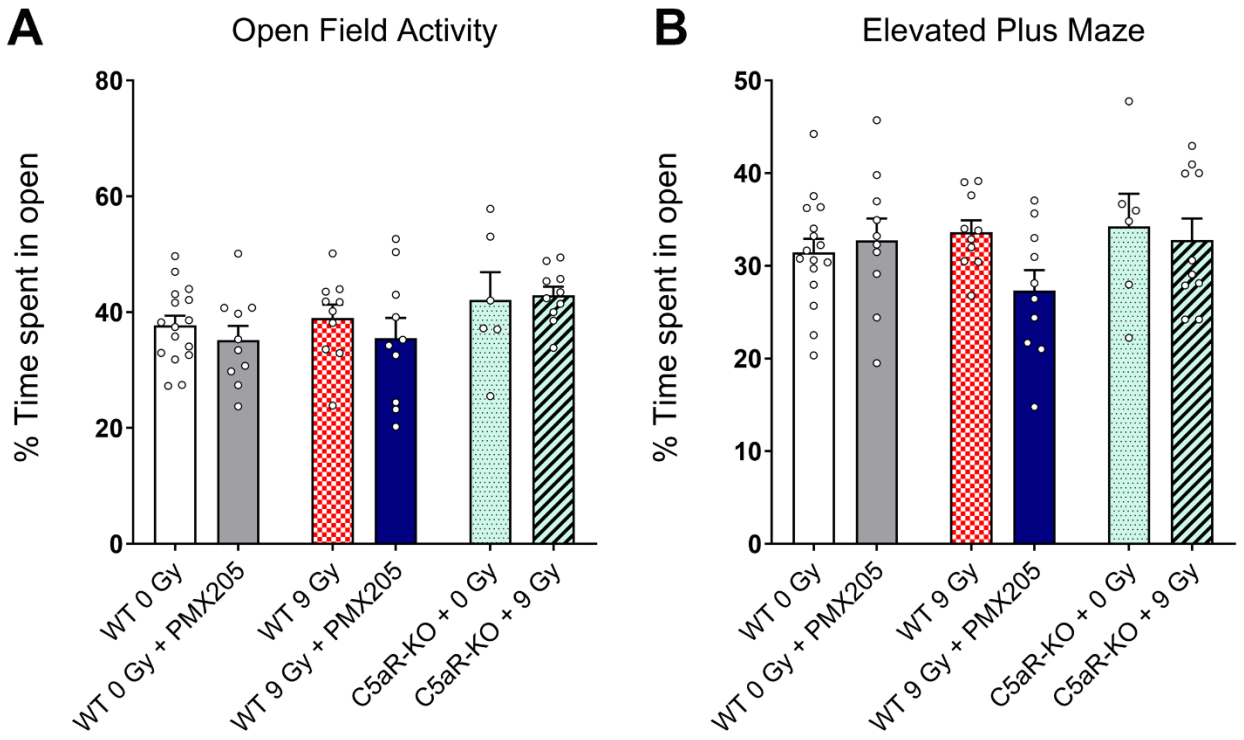


**Supplemental Figure S2.** Cranial irradiation, PMX205 treatment and C5aR1 KO did not the open field activity and anxiety-like behavior. No significant differences were observed between littermate 0 Gy or 9 Gy irradiated WT, WT mice treated with PMX205 and C5aR1 KO mice on the open field activity (percent time spent in open or central zone of an arena), and elevated plus maze (percent time spent in open arms) tests one-month post-irradiation. Data are presented as mean ± SEM (*N*=8-16 mice per group).

| STAR★METHODS | | |
|---|---|---|
| | | |
| **KEY RESOURCE TABLE** | | |
| | | |
| **REAGENT or RESOURCES** | **SOURCE** | **IDENTIFIER** |
| **Antibodies** | | |
| FITC anti-mouse CD45 | Biolegend | Cat. 157214; RRID: AB_2894427 |
| PE anti-mouse CD11b | Biolegend | Cat. 101208; RRID: AB_312791 |
| APC anti-mouse CD88 (C5aR1) | Biolegend | Cat. 135808; RRID: AB_10896758 |
| FITC anti-mouse/human CD11b | Biolegend | Cat. 101206; RRID: AB_312788 |
| PE anti-mouse Ly-6C | Biolegend | Cat. 128008; RRID: AB_1186132 |
| Rat anti Mouse CD68 | Bio-Rad | Cat. MCA1957; RRID: AB_322219 |
| Rabbit anti IBA1 | FUJIFILM Wako | Cat. 019-19741; RRID: AB_839504 |
| Rat anti-mouse CD88 (C5aR1) | FisherSci | Cat. MA1-81761; RRID: AB_929568 |
| Mouse anti C3d | Quidel | Cat. A702, RRID:AB_452517 |
| Rabbit anti GFAP | Covance | Cat. PRB-571C-100, RRID:AB_291696 |
| Mouse anti Synaptophysin | Sigma-Aldrich | Cat. S5768; RRID: AB_477523 |
| Mouse anti PSD95 | FisherSci | Cat. MA1-045; RRID: AB_325399 |
| Goat anti Rat Alexa Fluor 647 | Abcam | Cat. ab150159; RRID: AB_2566823 |
| Goat anti Rabbit Alexa Fluor 488 | FisherSci | Cat. a11008; RRID: AB_143165 |
| Goat anti Mouse Alexa Fluor 647 | Abcam | Cat. ab150115; RRID: AB_2687948 |
| | | |
| **Biological Samples** | | |
| CT2A-Luc astrocytoma cells | Sigma-Aldrich | Cat# SCC195; RRID:CVCL_ZJ60 |
| GL261 glioblastoma cells | NCI-DTP | Cat# Glioma 261; RRID:CVCL_Y003 |
| | | |
| **Chemicals, peptides, and recombinant proteins** | | |
| Gibco™ DMEM (1X) + GlutaMAX™-I | FisherSci | Cat. 10-569-010 |
| Gibco™ FBS | FisherSci | Cat. 10-082-147 |
| Gibco™ Hibernate™-A Medium | FisherSci | Cat. A1247501 |
| Isospire™ (isoflurane) Inhalation Anesthetic | Dechra | N/A |
| Betadine® Surgical Scrub | Patterson Veterinary | Cat. 07-808-8897 |
| Hydrogen Peroxide, 30% (Certified ACS) | FisherSci | Cat. H325-500 |
| Normal Saline (Sodium Chloride) 0.9% | Patterson Veterinary | Cat. 07-800-9424 |
| Buprenorphine HCl (0.3 mg/ml) | MWI Health | N/A |
| VECTASHIELD® Antifade Mounting Medium | VectaShield | Cat. H-1000-10 |
| D-Luciferin, sodium salt | GoldBio | Cat. eLUCNA |
| Gibco™ DPBS (no magnesium, no calcium) | FisherSci | Cat. 14-190-144 |
| Iohexol (Omnipaque™) 350 mgI/ml | GE Healthcare | N/A |
| PMX205 | Dr. Trent Woodruff, Univ. of Queensland | N/A |
| DMSO | FisherSci | AAJ66650K2 |
| Virkon, premixed spray bottle | University Laboratory Animal Resources | N/A |
| Sodium Chloride, NaCl | Sigma-Aldrich | S9888 |
| Heparin sodium salt from porcine intestinal mucosa | Sigma-Aldrich | Cat. H3149 |
| Gibco™ HBSS (no magnesium, no calcium) | FisherSci | Cat. 14-175-079 |
| Collagenase from Clostridium histolyticum | Sigma-Aldrich | Cat. C0130-500MG |
| Nα-Tosyl-L-lysine chloromethyl ketone hydrochloride | Sigma-Aldrich | Cat. T7254-100MG |
| DNAse 1 | Zymo | E1011-A |
| Gibco™ HEPES (1M) | FisherSci | Cat. 15-630-080 |
| Gibco™ RPMI 1640 Medium, GlutaMAX™ Supplement | FisherSci | Cat. 61870036 |
| Cytiva Percoll™ Centrifugation Media | FisherSci | Cat. 45-001-748 |
| Gibco™ DPBS (10X), no calcium, no magnesium | FisherSci | Cat. 14-200-075 |
| GenClone 25-508 DPBS, 1X, without Ca, Mg, Phenol Red, 0.1um Sterile Filtere | Genesee Scientific | Cat. 25–508 |
| Invitrogen™ eBioscience™ Flow Cytometry Staining Buffer | FisherSci | Cat. 501128916 |
| Paraformaldehyde | Sigma-Aldrich | Cat. 158127 |
| Sodium azide | Sigma-Aldrich | Cat. S2002 |
| Sucrose | Sigma-Aldrich | Cat. S7903 |
| Tissue-Tek® O.C.T. Compound | VWR | Cat. 25608-930 |
| Tris-buffered Salin (10X TBS) | Bioland Scientific | Cat. TBS01-03 |
| Triton™ X-100 Surfact-Amps™ Detergent Solution | FisherSci | Cat. 85111 |
| Phosphate-Citrate Buffer with Sodium Perborate | Sigma-Aldrich | Cat. P4922 |
| TWEEN® 20 | Sigma-Aldrich | Cat. 655204 |
| Boric acid | Sigma-Aldrich | Cat. B0394 |
| Normal Goat Serum | Jackson ImmunoReasearch | Cat. 005-000-121 |
| Bovine Serum Albumin | Sigma-Aldrich | Cat. 05470 |
| Methanol (Certified ACS), Fisher Chemical™ | FisherSci | Cat. A412500 |
| TRIzol™ Reagent | FisherSci | Cat. 15596026 |
| M-MLV Reverse Transcriptase | Promega | Cat. M170A |
| RT 5X buffer | Promega | Cat. M531A |
| Oligo (dT) 18 Primer | FisherSci | Cat. S0131 |
| dNTP Set (100 mM) | FisherSci | Cat. 10297018 |
| RNasin® Ribonuclease Inhibitor | Promega | Cat. N2511 |
| DL-Dithiothreitol (DTT) | FisherSci | Cat. 707265ML |
| DEPC-Treated Water | FisherSci | Cat. AM9920 |
| | | |
| **Critical commercial assays** | | |
| Direct-zol RNA Miniprep | Zymo | Cat. R2050 |
| Applied Biosystems™ TaqMan™ Universal PCR Master Mix, no AmpErase™ U | FisherSci | Cat. 4324018 |
| TaqMan Gene Expression Assays (Assays ID: GAPDH Mm99999915_g1) | FisherSci | Cat. 4331182 |
| TaqMan Gene Expression Assays (Assays ID: CD88 Mm00500292_s1) | FisherSci | Cat. 4331182 |
| | | |

| REAGENT or RESOURCES | SOURCE | IDENTIFIER |
|---|---|---|
| **Software and algorithms** | | |
| Living Image Software | Revvity (Perkin Elmer) | Cat.128110 |
| OsiriX Lite Software | Pixmeo SARL | N/A |
| Noldus EthoVisionXT 17 Tracking Software | Noldus | N/A |
| FreezeFrame | Coulbourn Instruments | N/A |
| Imaris 10.0 | Oxford Instruments | N/A |
| | | |
| **Other** | | |
| RC2 – Rodent Circuit Controller | VetEquip | Cat. 922100 |
| Ultra Precise Digital Just for Mouse Stereotaxic Instrument | Stoelting | Cat. 51730UD |
| Sterile Alcohol Prep Pads | FisherSci | Cat. 06-669-62 |
| Feather™ Single-Use Scalpels | FisherSci | Cat. 08-927-5B |
| 10 µL Microliter Syringe Model 701 N | Hamilton | Cat. 80300 |
| Pivetal® WebCryl™ Sutures | Patterson Veterinary | Cat. 07-891-0161 |
| 3M™ Vetbond™ Tissue Adhesive Bottle | Patterson Veterinary | Cat. 07-805-5031 |
| Fisherbrand™ Superfrost™ Plus Microscope Slides | FisherSci | Cat. 22-037-246 |
| IVIS Lumina III in vivo Imaging System | Revvity (Perkin Elmer) | Cat. CLS136334 |
| SmART+ X-ray Irradiator | Precision, Inc. | N/A |
| Noldus EthoVisionXT 17 Video Capture Hardware System | Noldus | N/A |
| C1000 Touch™ Thermal Cycler with Dual 48/48 Fast Reaction Module | Bio-Rad | Cat. 1851148 |
| Microm Cyrostar HM525 NX Cryostat | Epredia | Cat. 95-664-0EC70 |

## RESOURCE AVAILABILITY

### Lead contact

For additional information and request of resources and reagents, please direct correspondence to the lead contact, Munjal Acharya (macharya@uci.edu).

### Materials availability

This study did not generate any new unique reagents.

### Data and code availability

- All data reported in this paper will be shared by the lead contact upon request.
- This paper does not report the original code.
- Any additional information required to reanalyze the data reported in this paper is available from the lead contact upon request.

## EXPERIMENTAL MODEL AND SUBJECT DETAILS

### Mice

All animals used in this study were cared for in accordance with the guidelines provided by NIH and approved by the Institutional Animal Care and Use Committee (IACUC) at University of California, Irvine.

Wild-type male mice, aged 15-16 weeks (C57BL/6J, RRID:IMSR_JAX:000664) were obtained from The Jackson Laboratory and housed in standard conditions (20 °C±1 °C; 70% ± 10% humidity;12h:12h light and dark cycle) in groups of 2-5 mice per cage. Homozygous C5aR1 KO males (C5aR -/-), aged 15-16 weeks, were bred in-house. The progenitors were graciously provided by Dr. Rick A. Wetsel, University of Texas Health Science Center, Houston. Dr. Wetsel had previously developed a C5aR -/- transgenic mouse model via targeted deletion of the C5a receptor 1 gene (PMID: 18063050). The in-house breeding colony was maintained and expanded via selective inbreeding to produce homozygous offspring, and the genotype of digested tail clips or ear punches was confirmed by PCR. All C5aR1 KO mice were housed in standard conditions (20 °C±1 °C; 70% ± 10% humidity;12h:12h light and dark cycle) in groups of 2-5 mice per cage. For both wild-type and C5aR1 KO, littermates were randomly assigned to experimental groups. Groups that underwent intracranial tumor induction and/or cranial radiation therapy (RT).

## METHOD DETAILS

### Experimental design

C5a receptor inhibition and its effects on cognition in the irradiated brain were first studied in non-cancer-bearing mouse models, either with pharmacological intervention via cyclic hexapeptide C5a inhibitor PMX205 or through genetic ablation with the C5aR1 Knockout (KO) transgenic mouse model. For this study, 15-16 weeks male mice were divided into the following groups: 1) WT mice receiving 0 Gy or 9 Gy cranial radiation therapy (CRT) with or without PMX205 treatment and 2) C5aR1 KO mice receiving 0 Gy or 9 Gy CRT. One month post-treatment, cognitive function testing was performed, followed by euthanasia and tissue harvesting. For the tumor-bearing model, WT C57Bl6 male mice (15-16 weeks old) were divided into the following groups and applied to both the astrocytoma (CT2A-Luc) and glioblastoma (GL261) tumor types: Tumor + Vehicle, Tumor + RT, Tumor + PMX205, and Tumor + RT + PMX205. Tumor growth and animal health were monitored over the period of one- to two-month post-treatment. A cohort of mice underwent cognitive function testing at three- to four weeks post-treatment.

### Preparation of mouse glioma cells for tumor induction

CT2A-Luc mouse astrocytoma cells (Sigma-Aldrich, Cat. SCC195, RRID:CVCL_ZJ60 ) and GL261 mouse glioblastoma cells (NCI-DTP, Cat. Glioma 261, RRID:CVCL_Y003) were cultured in monolayer with Gibco™ DMEM (1X) supplemented with GlutaMAX™-I (FisherSci, Cat. 10-569-

010) and 10% Gibco™ FBS (FisherSci, Cat. 10-082-147) at 37°C and 5% $CO_2$. For surgical preparation, CT2A-Luc and GL261 cell cultures were first trypsinized with Gibco™ TrypLE™ Express Enzyme (FisherSci, Cat. 12-605-010), spun down at 300g for 5 minutes, resuspended in Gibco™ Hibernate™-A Medium (FisherSci, Cat. A1247501) and kept on ice until the implantation. Successful tumor induction in mouse subjects required a minimal cell 2,000 cells per brain, injected in a total volume of 2 µl per animal.

**Stereotaxic intracranial Implantation of mouse glioma cells**

Experiment groups undergoing tumor induction were first anesthetized with 2.0% v/v inhalant isoflurane (Dechra) delivered at 1000 cc/min ± 10% with a passive scavenging anesthesia system (VetEquip, Cat. 922100). Mice were subsequently shaved with an electric trimmer, mounted to a digital stereotaxic rig (Stoelting, Cat. 51730UD) and kept under anesthesia with 2.0% inhalant isoflurane at 500 cc/min ± 10%. The shaved scalp was prepped with Betadine® Surgical Scrub (Patterson Veterinary, Cat. 07-836-3379) followed by Sterile Alcohol Prep Pad (FisherSci, Cat. 06-669-62); this was repeated two more times. A single midline sagittal incision was made with a scalpel (FisherSci, Cat. 08-927-5B) and the underlying soft tissue was treated with 3% hydrogen peroxide (FisherSci, Cat. H325-500) to expose bregma, which is the origin point for stereotaxic coordinates in mice. The coordinates for the tumor cell implantation were anterior-posterior (AP) +1.54 mm, medial-lateral (ML) +2.00 mm, and dorsal-ventral (DV) -3.00 mm. The AP-ML coordinates were demarcated with a fine-tip pen, and a bone drill was used to create an opening in the cranium. A 10 µl Hamilton syringe with a cemented needle (Hamilton, Cat. 80300) was used to draw up 2 µl of the tumor cell suspension. The dose was injected at DV -3.00 mm in two stages, with a 60-second pause after the first microliter and a six-minute pause after the second microliter. The needle was then withdrawn in a stepwise manner from DV -2.00 mm to -1.00 mm, with a 60-second pause at each step to prevent the backflow of the tumor suspension. The incision was closed in an interrupted pattern with size 6-0 polyglactin-coated sutures (Patterson Veterinary, Cat. 07-891-0161) and tissue adhesive (Patterson Veterinary, Cat. 07-805-5031). Animals were placed in a recovery cage on a heating pad and monitored until they gained consciousness, during which animals received a 1.0 ml intraperitoneal injection of saline (0.9% NaCl, Patterson Veterinary, Cat. 07-800-9424). Post-surgical analgesic care consisted of a subcutaneous injection of Buprenorphine HCl (MWI Health) diluted in saline to 0.1 mg/kg body weight. This was delivered once at the end of the surgery and then again at 12 hours later.

**Tumor growth measurements for the CT2A-Luc- and GL261-implanted animals**

Astrocytoma (CT2A-Luc) tumor growth was measured via bioluminescence imaging (BLI). Animals received a 200 µl intraperitoneal injection of the bioluminescent reporter substrate luciferin, which was prepared as a 15 mg/ml stock solution from D-Luciferin, sodium salt (GoldBio, Cat. eLUCNA) and Gibco™ DPBS (no calcium, no magnesium, FisherSci, Cat. 14-190-144). Injected mice were then anesthetized using isoflurane (as above) and placed in a prone position inside the IVIS Lumina III *in vivo* Imaging System (Revvity, Perkin Elmer, Cat. CLS136334). The enzymatic activity of the luciferase expressed by the CT2A-Luc cells was captured, visualized, and quantified with the accompanying Living Image Software (Revity, Perkin Elmer, Cat.128110). The time from injection to image capture was optimized by performing serialized acquisitions on two subjects until a peak emittance was observed at approximately 12-14 minutes post-injection. This time interval was maintained for all subsequent subjects and weekly time points.

Glioblastoma tumor growth was tracked using cone-beam computed tomography (CBCT) using the SmART+ image-guided X-ray research irradiator (Precision, Inc.). To enhance soft-tissue contrast, 50 mg of iohexol (Omnipaque™ 350 mgI/ml, GE Healthcare) was injected retro-orbitally into anesthetized mice immediately prior to imaging. DICOM images were analyzed with OsiriX Lite Software (Pixmeo SARL) to calculate the tumor size.

**Cranial radiation therapy (CRT)**

CRT was administered to the WT and C5aR1 KO mice, to the assigned tumor groups approximately 7-9 days post-tumor induction using the SmART+ X-ray irradiator. A total of 9 Gy was delivered using a 0.3mm Copper filter, a 10×10 mm fixed collimator, and a photon spectrum of 225 kVp at 20 mA for 1 minute and 50 seconds. The treatment was delivered in 2 equal doses of 4.5 Gy in series on the same day in the sagittal plane to minimize damage to tissue outside the region of interest.

**PMX205 preparation and administration**

The cyclic hexapeptide C5a inhibitor PMX-205 was manufactured at Mimotopes (Australia) in consultation with Drs. Trent Woodruff and Richard Clark, The University of Queensland, Brisbane. The drug IC50 activity was confirmed in the Woodruff lab before shipping to the U.S. An initial 10 mg/ml stock solution comprised 50% DMSO (FisherSci, Cat. AAJ66650K2) in Milli-Q $H_2O$. The PMX205 treatment paradigm consisted of one week of daily subcutaneous injections at 1 mg/kg body weight and a month-long consumption of 100 µg/day (or 20 µg/ml) in the drinking water, both of which began 48 hours post-CRT. Water consumption was tracked weekly, and bottles were rotated thrice weekly to encourage complete fluid intake.

**Object recognition memory (ORM) and object location memory (OLM)**

Object recognition memory (ORM) and object location memory (OLM) tests depend on intact hippocampal, perirhinal cortex, and medial prefrontal cortex functions (2,3). The ORM task evaluates episodic memory by measuring animal's preference to explore novel objects, whereas the OLM task evaluates spatial recognition. For both tasks, the setup includes testing rooms equipped with appropriate lighting (~50 Lux), four square arena boxes, camera recording hardware (Noldus), and tracking software (EthoVision XT 17). The ORM and OLM tasks were conducted as described previously (1 and 4, respectively). Briefly, for the ORM task, the mice were habituated in open field arena boxes (33 × 33 × 33 cm) with a thin layer of bedding and without any objects for 10 minutes each run in 3 consecutive days. For the ORM task, the familiarization phase allowed the mice to explore two identical plastic toys that were magnetically secured in place 16 cm apart from opposing corners for 5 minutes. After a 5-minute interval in their cages, a novel object replaced one of the familiar objects (both toys were thoroughly cleansed with 10% ethanol and dried). Mice were then returned to the arena boxes and allowed to explore for 5 minutes. Following the test phase, all mice were returned to their home cage. The OLM task was conducted the following week after the ORM task. Mice were allowed to familiarize themselves with the testing room and open field arena boxes (33 × 33 × 33 cm) with a water-resistant, matte finish blue tape down the inside wall of the arena boxs and a layer of bedding. Mice were allowed to explore two identical toys that were placed 16 cm apart from each other for 5 minutes. Following similar steps from the ORM task, mice were returned to the home cage for 5 minutes while the objects were cleansed with 10% ethanol. One object was then moved to a new location inside the box (novel place), 16 cm from the opposite corner of the other toy, which remained in its former spatial location (familiar phase). Mice were returned to arena boxes and allowed to explore for 5 minutes. Mice behavior from all phases was recorded, and the "head direction to zone" function from Ethovision software was utilized to track the exploration time. Furthermore, to ensure unbiased analysis, time spent interacting (nose within 2 cm) with familiar vs novel (or relocated) objects was scored by observers blinded to the experimental conditions. The discrimination index (DI) was calculated for each animal using the equation: ([Novel object or location exploration time/Total exploration time] – [Familiar object or location exploration time/Total exploration time]) × 100.

**Elevated plus maze (EPM)**

The EPM test is a measure of anxiety that consists of two bisecting platforms in the shape of a plus sign constructed some distance off the ground, with one open arm with no walls or roof and one closed arm that consists of high barriers and a darker environment (7). Prior to testing, the floor and walls of the maze were cleaned with odor-elimination disinfectant (Virkon, University Laboratory Animal Resources, UCI) and then dried with paper towels. Each mouse subject was placed at the intersection of both arms and allowed to explore for a duration of 5 minutes. Testing was recorded with the same camera hardware and analyzed with accompanying tracking software (Noldus). The ratio of time spent in the open versus closed arms was then compared across experimental groups as a proxy for anxious behavior.

**Fear extinction memory**

To determine if C5a inhibition or knockdown in the irradiated brain affects amygdala-hippocampal circuit-dependent fear conditioning learning and fear memory consolidation, we performed fear extinction behavior reliant on hippocampal function (5,6). Testing occurred in a behavioral conditioning chamber (17.5 × 17.5 × 18 cm, Coulbourn Instruments) with parallel steel grid shock floors (3.2 mm diameter slats, 8 mm spacing), and a waste collection tray sprayed with 10% vinegar. For the initial fear conditioning phase (day 1), mice were allowed to habituate to the chamber for two minutes. Three pairings of an auditory conditioned stimulus (16 kHz tone, 80 dB, lasting 120 sec; CS) co-terminating with a foot shock unconditioned stimulus (0.6 mA, 1 sec; US) were presented at two-minute intervals. On the following three days of extinction training (days 2-4), mice were initially habituated to the same context for two minutes before being presented with 20 non-US reinforced CS tones (16 kHz, 80 dB, lasting 120 sec, at 5 sec intervals). On the final day of fear testing (day 5), mice were presented with only three non-US reinforced CS tones (16 kHz, 80 dB, lasting 120 sec) at two-minute intervals in the same context. Freezing behavior was recorded with a camera mounted above the chamber and scored by an automated measurement program (FreezeFrame, Coulbourn Instruments). FreezeFrame algorithms calculated a motion index for each frame of the video, with higher values representing greater motion. An investigator blinded to the experimental groups set the motion index threshold representing immobility for each animal individually based on identifying a trough separating low values during immobility and higher values associated with motion. Freezing behavior was defined as continuous bouts of one second or more of immobility. The data for the percentage of time each mouse spent freezing was then calculated for the final day of the extinction test.

**Isolation of immune cells from brains and blood**

On the day of analysis, mice blood and whole brains were freshly collected. Mice were deeply anesthetized with 2% isoflurane v/v (inhalation, Dechra) prior to the terminal blood collection and intracardiac perfusion. The heart was exposed after the opening of the thoracic cavity, and blood was carefully drawn via cardiac puncture (volume ~ 200uL) using a 28G needle and immediately placed in tubes coated with saline (0.9% NaCl, Sigma-Aldrich Cat. S9888) containing 20 U/ml heparin (Sigma-Aldrich, Cat. H3149) in ultra-pure water (Milli-Q $H_2O$) at room temperature (rt) for later processing. Next, intracardiac perfusion using a peristaltic pump was performed using ice-cold saline with 10 U/ml of heparin (Sigma-Aldrich) to prevent blood clotting. Brains and spleens were immediately collected and placed in separate tubes filled with Gibco™ HBSS (FisherSci, Cat. 14-175-079) with 10% Gibco™ FBS (FisherSci, Cat. 10-082-147) on ice. Once all the samples were collected, brains were transferred to tubes containing digestion buffer (0.05% Collagenase D Sigma-Aldrich Cat. C0130-500MG; 0.1µM TLCK, Sigma-Aldrich Cat. T7254-100MG, 10µg/mL DNAse 1, Zymo Cat. E1011-A; 10mM HEPES, FisherSci Cat. 15-630-080 in HBSS, FisherSci) and mechanically dissociated by mincing and incubated at 37ºC for 20 minutes. Minced brain tissues were sequentially forced through a 70 µm cell strainer and centrifuged to discard the supernatant layer. Cells were then resuspended and mixed in 37% Percoll gradient (prepared Isotonic percoll by mixing Percoll, FisherSci Cat. 45001748, with 5% 10X DPBS, FisherSci Cat.14-200-075; diluted to 37% Percoll using RPMI, FisherSci Cat. 61870036, with 5% FBS, FisherSci) and centrifuged at 400g, 4ºC for 25 minutes with brake and acceleration off only for this step. Myelin from the top opaque white layer was removed and discarded. Immune cells of interest residing in the pellet at the bottom layer were washed in 1x PBS (100 mM, pH 7.4) at 300g, 4°C for 3 minutes, and the supernatants were discarded. The pellets containing cells of interest were resuspended in FACS buffer (1X DPBS, Genesee Scientific Cat. 25-508; 2% FBS, FisherSci) that were ready to be stained for flow cytometry. Spleens were crushed between two glass slides (FisherSci Cat. 22-037-246) and transferred to tubes filled with FACS buffer. Samples were centrifuged (10000g, 4ºC for 5 minutes), supernatant was discarded, and samples were incubated with red blood cell lysis buffer (FisherSci Cat. 501128916) at rt for 5 minutes. Samples were then washed, filtered through 70 µm cell strainer, centrifuged and collected from the pellet. Blood samples were incubated in the red blood cells lysis buffer in the dark for 15 minutes; samples were washed and centrifuged (500g, at rt for 5 minutes, twice) and resuspended in FACS buffer and ready to be stained for flow cytometry.

**Flow Cytometry**

Single-cell suspension from brains, blood, and spleen were divided into individual FACS tubes; samples were washed and resuspended in 30 µL of FACS buffer and incubated with antibodies. Brain and spleen cells were stained with 1 µL from each FITC anti-mouse CD45 (Biolegend, Cat. 157214), PE anti-mouse CD11b (Biolegend, Cat. 101208), APC anti-mouse CD88 (Biolegend, Cat. 135808) antibodies and DAPI (1µmol/L, FisherSci Cat. D1306) in the dark at rt for 30 minutes. Cells from blood samples were stained with 1µL from each FITC anti-mouse CD11b (Biolegend, Cat. 101206), PE anti-mouse Ly6-C (Biolegend, Cat. 128008), and APC anti-mouse CD88 (Biolegend, Cat. 135808) in the dark at rt for 20 minutes. Each sample was washed with 2mL of 1X DPBS (300g, 4$^{o}$C for 3 minutes) and then 300µL of FACS buffer was added to each tube. Samples were acquired on LSRFortessa (BD Bioscience) or a FACSCelesta (BD BioScience) flow cytometer and data was analyzed using FlowJo software (Tree Star).

**RNA extraction and PCR analysis**

Brains from each group that were snap frozen in liquid nitrogen were homogenized in TRIzol reagent (FisherSci Cat. 15596026). RNA from the homogenized sample were extracted and purified following precisely the recommendations described in the Direct-zol RNA Miniprep with an additional step of DNAse treatment (Zymo, Cat. R2050). Approximately 0.5µg of RNA from each sample were reverse-transcribed to become cDNA by mixing with the master-mix (200 u/µL M-MLV Reverse Transcriptase, Promega Cat. M170A, 1.25µM RT 5X buffer, Promega Cat. M531A, 0.5mg/mL Oligo (dT) 18 Primer, FisherSci Cat. S0131, 100mM dNTP, FisherSci Cat. 10297-018, 40 u/µL RNAsin, Promega Cat. N2511, 2.5µM DTT FisherSci Cat. 707265ML in DEPC Water, FisherSci Cat. AM9920) under these specific thermocycler conditions (Bio-rad Cat. 1851148): 38$^{o}$C for 60 minutes; 90 $^{o}$C for 5 minutes. RT-PCR reactions was performed using pre-designed Taqman probes (FisherSci Cat# 4453320; Assay ID: GAPDH: Mm99999915_g1; CD88:Mm00500292_s1) and the Taqman Universal Master Mix, no AmpErase UNG (Thermo Fisher Scientific, Cat. 4324018) followed precisely the thermocycler parameters according to the manufacturer's recommendation. Gene expression data are presented as $2^{-(\Delta\Delta Ct)}$ values.

**Fixed brains collection**

Mice inhaled isoflurane and were euthanized using intracardiac perfusion technique using ice-cold saline (0.9% NaCl with 10 U/ml heparin) until the liver turned slightly pale and the venous outflow was clear. Saline with heparin (10 U/ml) was then replaced with 4% paraformaldehyde (Sigma-Aldrich Cat. 158127, pH 7.4) and steadily perfused until the animal body became stiff. Whole brains were extracted and soaked in 4% PFA overnight and switched to store in PBS-

0.05% sodium azide (Sigma-Aldrich Cat. S2002, pH 7.4). Brains were immersed in a sucrose gradient (10% to 30% w/v, Sigma Cat. S7903, pH 7.4) to dehydrate the brains and avoid crystal formation that could disrupt the brain structure during cryo-sectioning. Whole brains were then embedded in OCT compound (VWR Cat. 25608903) and cryo-sectioned (floating 30µm, coronal) using a cryostat (Microm Cryostar HM525 NX, Epredia, MI). Brain sections were stored in 24-well plates in PBS (100 mH, pH 7.4 with 0.05% Sodium Azide (Sigma-Aldrich, pH 7.4) for the IHC experiments.

**Immunohistochemistry**

Floating frozen brain sections were collected from each group (two sections with visible mid hippocampus region per brain, four brains per group) for immunohistochemistry. For synaptophysin, PSD95, C5aR1 and CD88-IBA1 staining, tissue sections were washed in 1x TBS (100 mM, pH 7.4; diluted with MilliQ-Water from 10x TBS, Bioland Scientific Cat. TBS01-03) three times (5 minutes each) and Tris-A solution (0.1% Triton-X, FisherSci Cat. 85111, in 1x TBS, pH 7.4) at rt for 10 minutes. Antigen retrieval for tissues from synaptophysin staining was facilitated by incubating in citrate buffer at 10 mM with 0.05% Tween-20 (pH 6.0, Sigma-Aldrich Cat. P4922 and Cat. 655204, respectively) at 70ºC for 30 minutes and recovery in borate buffer (100mM, pH 8.5, Sigma-Aldrich Cat. B0394) at rt for 10 minutes and washed with 1x TBS (2 washes, 5 minutes each). Prior to staining with primary antibodies, sections were incubated in blocking solution with each respective secondary antibody host. This included 3% normal goat serum, NGS with 1% Bovine Serum Albumin or BSA in Tris-A buffer for synaptophysin; 4% BSA in Tris-A buffer for PSD95; 3% NGS in Tris-A buffer for CD88 (C5aR1) and CD68/IBA1 markers (NGS, Jackson ImmunoResearch Cat. 005-000-121; BSA, Sigma-Aldrich Cat. 05470) at rt for 45 minutes. Sections were incubated in primary antibodies at 4ºC overnight (1:1000 for mouse anti-synaptophysin, Sigma Cat. S5768, in 3% NGS and 1% BSA in Tris-A buffer); 1:1000 for mouse anti-PSD95 (Fisher Scientific Cat. MA1-045, with 2% BSA in Tris-A buffer); 1:500, rat anti-mouse CD88 (FisherSci Cat. MA1-81761), combined with 1:500 rabbit anti-IBA1 (FUJIFILM Wako Cat. 019-19741, with 3% NGS in Tris-A) for CD88-IBA1 dual stain,. Sections were placed at room temperature for 1 hour the next day before staining for secondary antibodies. Sections were washed with 1x TBS (3 times, 5 minutes each) and then transferred to secondary antibodies to incubate at room temperature for one hour to visualize the target antigens (1:1000 Goat anti-mouse Alexa Fluor (AF) 647, Abcam Cat. ab150115, for both synaptophysin and PSD95 markers;1:750 goat anti-rat AF 647, Abcam Cat. ab150159, for CD88 marker, and 1:500 goat anti-rabbit AF 488, Fisher Scientific Cat. a11008, for IBA1 marker). Lastly, brain sections were

counterstained with DAPI nuclear dye (1µmol/L, FisherSci Cat. D1306) in 1x TBS at room temperature for 15 minutes. Stained sections were then washed with 1x TBS (2 times, 5 minutes each) and mounted on superfrost slides (FisherSci Cat. 22-037-246) using VectaShield antifade mounting medium (VectaShield Cat. H-1000-10). Staining for C3d/GFAP markers followed the exact similar steps as synaptophysin as described above with a minor change of buffer use (1x PBS, FisherSci) and antibodies. Primary antibodies comprised of 1:750 mouse anti-C3d (Quidel Cat. A702), and 1:500 rabbit anti-GFAP (Covance Cat. PRB-571C-100). The secondary antibodies were 1:1000 goat anti-mouse AF 647 (Abcam Cat. ab150115) and, 1:500 goat anti-rabbit AF 488 (FisherSci Cat. a11008).

Immunohistochemistry staining for CD68-IBA 1 markers follow similar steps above with some minor changes. First, brain sections were washed with PBS with 0.3% Tween 20 (Sigma-Aldrich) three times (5 minutes each) and then incubated in 3% hydrogen peroxide solution (FisherSci Cat. H325-500), with 1% Methanol (FisherSci Cat. A412500) in 1x PBS (FisherSci) at room temperature for 30 minutes to block any endogenous peroxidase activity. Sections were washed in 1x PBS (3 times, 5 minutes each) prior to incubating in blocking solution (4% BSA in PBS with 0.33% Tween-20, Sigma-Aldrich) at room temperature for 30 minutes. Brain sections were then incubated in primary antibodies at 4$^{o}$C overnight (1:500, rat anti-mouse CD68, Bio-rad Cat. MCA1957, combined with 1:500 rabbit anti IBA-1, FUJIFILM Wako Cat. 019-1974) with 1% BSA in PBS with 0.3% Tween-20 buffer. Sections were washed and stained in secondary antibodies at room temperature for one hour (1:1000, goat anti-rat AF 647, Abcam Cat. ab150159, for CD68 marker, and 1:500, goat anti-rabbit AF 488, FisherSci Cat. a11008, for IBA1 marker). Sections were washed and counterstained with DAPI nuclear dye (1µmol/L, FisherSci Cat. D1306) and mounted on superfrost slides (FisherSci Cat. 22-037-246) using VectaShield antifade mounting medium (VectaShield Cat. H-1000-10).

**Confocal microscopy and 3D algorithm-based volumetric quantification**

Immunostained brain sections were imaged at high resolution (1024p) at 0.5 µm thick z stacks using a laser-scanning confocal microscope (Nikon AX) with a 40x oil-immersion objective lens. High-resolution images were deconvoluted and 3D volume surfaces were created for each antigen of interest using Imaris, an image analysis software (Oxford Instruments, see PMID 33323383 for details). For synaptophysin and PSD95, the surface volumes of synaptic puncta were obtained and analyzed. For CD68/IBA1 and C5aR1/IBA1, co-localization volumetric between the surfaces of two markers for each stain was determined and analyzed. All

immunostained image analyses were conducted using automated batch processing, which uniformly applied the parameters to all images to obtain unbiased analyses.

## STATISTICAL ANALYSIS

Statistical analyses were performed to confirm overall significance (GraphPad Prism, v8.0, RRID: SCR_002798). For the analysis of C5aR KO, PMX205 treatment, and cranial irradiation, two-way ANOVA or repeated measures ANOVA, and Bonferroni's multiple comparisons test were performed. For the tumor studies, P values were derived from the Mann-Whitney *U* test or long-rank test for survival studies. All results are expressed as the mean values ± SEM. All analyses considered a value of $P \leq 0.05$ to be statistically significant.

## REFERENCES (for METHODS)


1. Acharya MM, Baulch JE, Klein PM, Baddour AAD, Apodaca LA, Kramar EA, et al. New Concerns for Neurocognitive Function during Deep Space Exposures to Chronic, Low Dose-Rate, Neutron Radiation. eNeuro 2019;6. doi: 10.1523/ENEURO.0094-19.2019.
2. Barker GR, Bird F, Alexander V, Warburton EC. Recognition memory for objects, place, and temporal order: a disconnection analysis of the role of the medial prefrontal cortex and perirhinal cortex. J Neurosci 2007;27:2948-57
3. Barker GR, Warburton EC. When is the hippocampus involved in recognition memory? J Neurosci 2011;31:10721-31.
4. Parihar VK, Allen BD, Tran KK, Chmielewski NN, Craver BM, Martirosian V, Morganti JM, Rosi S, Vlkolinsky R, Acharya MM, Nelson GA, Allen AR, Limoli CL (2015c) Targeted overexpression of mitochondrial catalase prevents radiation-induced cognitive dysfunction 22(1):78-91. doi: 10.1089/ars.2014.5929.
5. Milad MR, Quirk GJ. Fear extinction as a model for translational neuroscience: ten years of progress. Annual review of psychology 2012;63:129-51.
6. Schubert I, Ahlbrand R, Winter A, Vollmer L, Lewkowich I, Sah R. Enhanced fear and altered neuronal activation in forebrain limbic regions of CX3CR1-deficient mice. Brain Behav Immun 2018;68:34-43.
7. Walf, A., Frye, C. The use of the elevated plus maze as an assay of anxiety-related behavior in rodents. Nat Protoc 2, 322–328 (2007). https://doi.org/10.1038/nprot.2007.44